SOME ASPECTS OF BLACK HOLE PHYSICS: SPHERICAL NULL AND TIMELIKE ORBITS, AND EVENT HORIZON DETECTION

A THESIS SUBMITTED TO
THE GRADUATE SCHOOL OF NATURAL AND APPLIED SCIENCES
OF
MIDDLE EAST TECHNICAL UNIVERSITY

BY

AYDIN TAVLAYAN

IN PARTIAL FULFILLMENT OF THE REQUIREMENTS
FOR
THE DEGREE OF MASTER OF SCIENCE
IN
PHYSICS

SEPTEMBER 2021

Approval of the thesis:

SOME ASPECTS OF BLACK HOLE PHYSICS: SPHERICAL NULL AND TIMELIKE ORBITS, AND EVENT HORIZON DETECTION

submitted by **AYDIN TAVLAYAN** in partial fulfillment of the requirements for the degree of **Master of Science in Physics Department, Middle East Technical University** by,

Prof. Dr. Halil Kalıpçılar
Dean, Graduate School of **Natural and Applied Sciences** ______________

Prof. Dr. Seçkin Kürkçüoğlu
Head of Department, **Physics** ______________

Prof. Dr. Bayram Tekin
Supervisor, **Physics, METU** ______________

Examining Committee Members:

Prof. Dr. Atalay Karasu
Physics, METU ______________

Prof. Dr. Bayram Tekin
Phyiscs, METU ______________

Prof. Dr. Tahsin Çağrı Şişman
Astronautical Engineering, UTAA ______________

Date: 08.09.2021

I hereby declare that all information in this document has been obtained and presented in accordance with academic rules and ethical conduct. I also declare that, as required by these rules and conduct, I have fully cited and referenced all material and results that are not original to this work.

Name, Surname: Aydın Tavlayan

Signature :

ABSTRACT

SOME ASPECTS OF BLACK HOLE PHYSICS: SPHERICAL NULL AND TIMELIKE ORBITS, AND EVENT HORIZON DETECTION

Tavlayan, Aydın
M.S., Department of Physics
Supervisor: Prof. Dr. Bayram Tekin

September 2021, 71 pages

In this thesis, some crucial aspects of black hole physics are investigated. Exact formulas relating the radius of the spherical photon orbits to the black hole's rotation parameter and the effective inclination angle of the orbit have been known only for equatorial and polar orbits up to now. In the first chapter, an infinite family of exact formulas is provided for non-equatorial orbits that lie between these extreme limits. The sextic polynomial equation in the photon radius, derived from the geodesic equations, is studied to arrive at these novel analytical solutions. In the second chapter, the method developed to investigate the spherical orbits is modified in order to analyze the timelike orbits of the massive particles. For both null and timelike orbits, some approximate solutions are derived with the help of the Lagrange-Bürmann theorem, which provides a great understanding of the behavior of particles in the vicinity of a black hole. In the last part, an invariant characterization of event horizons of black holes is provided. As already known, some judiciously chosen local curvature scalars can be used to invariantly characterize event horizons of black holes in $D > 3$ dimensions. However, they fail for the three-dimensional Bañados-Teitelboim-Zanelli (BTZ) black hole since all curvature invariants are constant. Here, an invariant characterization of the event horizon of the BTZ black hole using the curvature invariants of codimension one hypersurfaces, instead of the full spacetime, is provided. The method developed in this work is also applicable to black holes in generic dimensions, but is most efficient in three, four, and five dimensions. Four-dimensional Kerr, five-dimensional Myers-Perry, three-dimensional warped-anti-de Sitter, and the three-dimensional asymptotically flat black holes are given as examples.

Keywords: Spherical Photon Orbits, Lagrange-Bürmann Inversion theorem, Kerr Black Hole, Curvature Invariants, BTZ Black Hole

ÖZ

KARA DELİK FİZİĞİNİN BAZI ÖZELLİKLERİ: KÜRESEL IŞIK BENZERİ VE ZAMAN BENZERİ YÖRÜNGLER VE OLAY UFKU TESPİTİ

Tavlayan, Aydın
Yüksek Lisans, Fizik Bölümü
Tez Yöneticisi: Prof. Dr. Bayram Tekin

Eylül 2021 , 71 sayfa

Bu tezde, kara delik fiziğinin bazı önemli özellikleri araştırılmaktadır. Küresel foton yörüngelerinin yarıçapını kara deliğin dönüş parametresine ve yörüngenin efektif eğim açısına bağlayan kesin formüller şimdiye kadar sadece ekvator ve kutup eksenindeki yörüngeler için biliniyordu. Birinci bölümde, bu sınırlar arasında kalan, ekvator eksininde olmayan, yörüngeler için sonsuz bir kesin formül ailesi verilmiştir. Jeodezik denklemler kullanılarak türetilen foton yarıçapının altıncı derece polinom denklemi, bu yeni analitik çözümlere ulaşmak için incelenmiştir. İkinci bölümde, küresel yörüngeleri araştırmak için geliştirilen yöntem, kütleli parçacıkların zaman benzeri yörüngelerini analiz etmek için geliştirilmiştir. Hem ışık benzeri hem de zaman benzeri yörüngeler için, Lagrange-Bürmann teoreminin yardımıyla, karadeliğin çevresindeki parçacıkların davranışının iyi bir şekilde anlaşılmasını sağlayan bazı yaklaşık çözümler türetilmiştir. Son bölümde, kara deliklerin olay ufuklarının değişmez bir karakterizasyonu sağlanmıştır. Halihazırda bilindiği gibi, özel olarak seçilmiş bazı yerel eğrilik skalerleri, $D > 3$ boyutlu kara deliklerin olay ufuklarını değişmez bir şekilde karakterize etmek için kullanılabilir. Ancak, tüm eğrilik değişmezleri sabit olduğundan, üç boyutlu Bañados-Teitelboim-Zanelli (BTZ) kara deliği için başarısız olurlar. Burada, tam uzay-zaman yerine bir hiperyüzey eşboyutunun eğrilik değişmezleri kullanılarak, BTZ kara deliğinin olay ufkunun değişmez bir karakterizasyonu sağlanır. Bu çalışmada geliştirilen yöntem, genel boyutlardaki kara deliklere de uygulanabilir, ancak en verimli olanları üç, dört ve beş boyuttadır. Dört boyutlu Kerr, beş boyutlu Myers-Perry, üç boyutlu çarpık-anti-de Sitter ve üç boyutlu asimptotik olarak düz kara delikler örnek olarak verilmiştir.

Anahtar Kelimeler: Küresel Foton Yörüngeleri, Lagrange-Bürmann Değişim Teoremi, Kerr Kara Deliği, Eğrilik Değişmezleri, BTZ Kara Deliği

To my family

ACKNOWLEDGMENTS

My quest for black holes had started when I first read an interesting article in a popular science magazine about them when I was in high school. Almost ten years later, I had the opportunity to work with the writer of that article. Therefore, I would like to express my sincere gratitudes to my supervisor Prof. Dr. Bayram Tekin, for sparking my interest in this area from the ground up and for his guidance and encouragement about my research.

I would like to thank Prof. Dr. Atalay Karasu and Prof. Dr. Tahsin Çağrı Şişman for their precious advice and comments. I would like to thank Prof. Dr. Emine Ayşe Karasu and Prof. Dr. Seçkin Kürkçüoğlu for their great lectures, which helped me decide to pursue a career in theoretical physics.

I am thankful to all my friends for their help throughout this stressful process.

I acknowledge TÜBİTAK for the financial support during my graduate education through 2210-A scholarship program. Also, I would like to thank American Physics Society (APS) for giving me the right to use our articles "Exact formulas for spherical photon orbits around Kerr black holes" and "Event horizon detecting invariants" in this thesis.

Finally and most importantly, I would like to thank my family for their endless support.

TABLE OF CONTENTS

ABSTRACT v

ÖZ vii

ACKNOWLEDGMENTS x

TABLE OF CONTENTS xi

LIST OF TABLES xiv

LIST OF FIGURES xv

LIST OF ABBREVIATIONS xviii

CHAPTERS

1 INTRODUCTION 1

  1.1 A Brief History of Black Holes 1

  1.2 Outline 3

  1.3 Light Orbits 4

  1.4 Curvature Invariants 5

2 EXACT FORMULAS FOR SPHERICAL PHOTON ORBITS AROUND KERR BLACK HOLES 9

  2.1 Null Geodesics 9

  2.2 Equatorial and Polar Orbits 11

  2.3 Schwarzschild Black Hole 13

2.4 Spherical Photon Orbits 13

2.5 Approximate Solutions 18

3 SPHERICAL GEODESICS FOR MASSIVE PARTICLES 21

3.1 Timelike Geodesics 21

3.2 The Schwarzschild Limit 23

3.3 Zero Energy Solution 24

3.4 Non-Monotonic Behaviour at Nonzero Energy Values 27

3.5 The Unit Energy Situation 29

3.5.1 Equatorial Plane Solutions 30

3.5.2 Lagrange-Bürmann Method 31

3.6 Other Energy Values 32

3.6.1 Bound Orbits 32

3.6.2 Unbound Orbits 37

4 EVENT HORIZON DETECTING INVARIANTS 39

4.1 Curvature invariants of the hypersurface 39

4.2 BTZ Black Hole 40

4.3 Warped AdS_3 black hole 41

4.4 Two examples in 2+1 dimensions 43

4.4.1 Asymptotically flat solution of K-gravity 43

4.4.2 Rotating solution of K-gravity 43

4.5 Kerr Black Hole 44

4.6 4+1 Myers-Perry Black Hole 45

5 CONCLUSIONS 47

REFERENCES 49

APPENDICES

A DERIVATION OF SEXTIC POLYNOMIAL 55

B ABEL-RUFFINI THEOREM 57

C TSCHIRNHAUSEN TRANSFORMATION AND NESTED RADICALS . . 59

D DISCRIMINANT OF A POLYNOMIAL 61

E DERIVATION OF THE CRITICAL ANGLE 63

F LAGRANGE-BÜRMANN THEOREM 65

G EXPLICIT FORMS OF INVARIANTS OF THE WARPED AdS_3 BLACK HOLE 67

H EXPLICIT FORMS OF INVARIANTS OF THE KERR BLACK HOLE . . 69

I EXPLICIT FORMS OF INVARIANTS OF THE 4+1 MYERS-PERRY HOLE 71

LIST OF TABLES

TABLES

Table 2.1 Comparison of approximate and exact numerical results around the prograde orbit at the equator, $x_0 = x_+$. Approximation is done with the Lagrange-Bürmann expansion up to order $\mathcal{O}(\nu^5)$. 20

Table 2.2 Comparison of approximate and exact numerical results around the retrograde orbit at the equator, $x_0 = x_-$. Approximation is done with the Lagrange-Bürmann expansion up to order $\mathcal{O}(\nu^5)$. 20

Table 3.1 The prograde and retrograde orbits for different energy, k, inclination angle, ν, and rotation parameter, u, values. 29

Table 3.2 The error rates of the approximate solution obtained with the Lagrange-Bürmann method to the unit energy particle orbits. 32

Table 3.3 The error rates of the approximate solution obtained with the Lagrange-Bürmann method at the equatorial plane $\nu = 0$ for bound orbits. 35

Table 3.4 The error rates of the approximate solution obtained with the Lagrange-Bürmann method at the polar plane $\nu = 1$ for bound orbits. 37

Table 3.5 The error rates of the approximate solution obtained with the Lagrange-Bürmann method at the equatorial plane, $\nu = 0$ for unbound orbits. 38

Table 3.6 The error rates of the approximate solution obtained with the Lagrange-Bürmann method at the polar plane, $\nu = 1$ for unbound orbits. 38

LIST OF FIGURES

FIGURES

Figure 2.1 Real roots of the sextic polynomial are plotted as a function of the rotation parameter on the equatorial plane. 12

Figure 2.2 Real roots of the sextic polynomial are plotted as a function of the rotation parameter on the polar plane. 13

Figure 2.3 Real roots of the sextic are plotted as a function of the rotation parameter at the critical inclination angle. The root corresponding to the retrograde orbit is nonmonotonic in u while the other roots are monotonic. Note that the third and the fourth roots are double roots and lie inside the event horizon for the nonextremal black hole. 16

Figure 2.4 The z-component of the angular momentum per unit energy and black hole mass is plotted for the real roots at the critical point as a function of the rotation parameter. The root corresponding to the retrograde orbit with a negative angular momentum component has a nonmonotonic dependence on u. 16

Figure 2.5 Second derivative of R from (2.8) is given for the critical photon orbits: for the exterior roots, the second derivative is positive and hence they are unstable orbits just like the prograde, retrograde, and the polar orbits. For the interior double root, the second derivative vanishes, so that root is a saddle point. 17

Figure 2.6 The dimensionless "impact parameter" $\frac{L}{mE}$ with $L = \sqrt{L_z^2 + \mathcal{Q}}$ for the retrograde orbits at the critical inclination angle and at the equatorial plane are plotted. The equatorial retrograde orbit has the highest impact parameter and is monotonic in the rotation parameter, while the impact parameter of the critical retrograde orbit is nonmonotonic. 17

Figure 2.7 The dimensionless "impact parameter" for the critical and equatorial prograde orbits are nonmonotonic in the impact parameter and they are both smaller than those of retrograde orbits. 18

Figure 3.1 Behavior of the orbit of a particle with zero energy outside the event horizon for different rotation parameter, u, and inclination angle, ν, values. 25

Figure 3.2 The exterior orbit and the event horizon are plotted as a function of rotation parameter, u, at the $\nu = 0.2$ plane. 25

Figure 3.3 The exterior orbit and the event horizon are plotted as a function of rotation parameter, u, at the $\nu = 0.8$ plane. 26

Figure 3.4 Roots of the polynomial on the equatorial plane for unit energy are plotted as a function of the rotation parameter. 31

Figure 3.5 The graph of the discriminant of the polynomial with $\nu = 0$ and $u = 0.1$. 33

Figure 3.6 The graph of the discriminant of the polynomial with $\nu = 0$ and $u = 0.9$. 34

Figure 3.7 The graph of energy values, k, which make the discriminant vanish on the equatorial plane with respect to u. 34

Figure 3.8 The graph of the discriminant of the polynomial with $\nu = 1$ and $u = 0.1$. 36

Figure 3.9 The graph of the discriminant of the polynomial with $\nu = 1$ and $u = 0.9$. 36

Figure 3.10 The graph of energy values, k, which makes the discriminant vanish on the polar plane with respect to u. 37

LIST OF ABBREVIATIONS

BTZ black hole	Bañados-Teitelboim-Zanelli black hole

CHAPTER 1

INTRODUCTION

1.1 A Brief History of Black Holes

The black hole concept is one of the most important consequences of the revolution in physics in the first half of the twentieth century. During this paradigm shift, two groundbreaking theories were born: quantum theory and relativity theory. Both theories have had a substantial impact on science and changed the course of history. The most important common feature of these two theories is that, besides explaining the experimental results far better than the old classical theories, they lead to bizarre concepts that were unimaginable before. For example, for an eighteenth-century physicist working on classical mechanics, the knowledge of the position and the momentum is enough to describe the particle's motion. Nevertheless, one of the most famous principles of the quantum theory, the uncertainty principle, forbids someone to measure the exact position and the exact momentum values simultaneously and introduced statistical concepts instead into the field. Another example is black holes which is the main object of this thesis.

Even though physicists were able to construct the mathematical foundations of black hole physics after the introduction of the general relativity theory in 1915, the idea of a black hole goes back to earlier times. British scientist John Michell published an exciting paper and presented it in 1784 at Royal Society [1]. In his paper, he applied Newton's law of gravitation to a particle on the surface of a sphere and deduced that if the mass of the sphere is large enough, the escape velocity of the particle on the surface can exceed the speed of light. He concluded that "all light emitted from such a body would be made to return towards it, by its own proper gravity" [2].

Simultaneously, another scientist from another country has been independently developing the concept of black holes. In his famous book, "*Exposition du Systeme du Monde*," French scientist Pierre-Simon Laplace wrote, "The gravitation attraction of a star with a diameter 250 times that of the Sun and comparable in density to the earth would be so great no light could escape from its surface." [1]. This was just a verbal statement without any mathematical proof. Laplace proved his assertion in another paper published in 1799 in the journal, the "*Allgemeine Geographische Ephemeriden*" [1], [3]. Interestingly, Laplace was not convinced by his own proof and removed his assertion in later editions of his book.

Newton's theory of gravitation was highly successful at explaining observational phenomena. Trajectories of planets were calculated, and even a new planet, Neptune, was discovered with the help of deviations of the observed orbit from the theoretically anticipated orbit [4], [5]. However, there were some observations that the Newtonian gravitation could not explain. For example, there was an inconsistency between the observed precession of perihelia of Mercury and the theoretically expected value. At first, astronomers thought that there may be another planet that had not been observed yet, between the Sun and Mercury. Nevertheless, no such planet was found. This was one of the points at which Newtonian gravitation failed [6]. A new theory explaining gravitation was necessary.

After publishing the paper founding the special relativity in 1905, Albert Einstein started to work on a new, generalized relativity theory that can explain gravitation thoroughly even under extreme conditions. In a series of papers published between 1913-1916, Albert Einstein introduced the general theory of relativity. In 1915, he showed how his theory explains the precession of perihelia of Mercury successfully in a paper [7]. In the final days of 1915, Einstein received a letter written to show that there is an exact result of Einstein's field equations for a static spacetime. The letter was written by Karl Schwarzschild, and he published his result in 1916. The result had an interesting property. It possessed singularities at the origin of the spacetime and at a unique point, $r = 2m$, where r is the radial coordinate of the spacetime, m is the mass of the black hole and gravitational constant, G, and the speed of light in vacuum, c, were equal to one due to the geometric unit system, today known as the Schwarzschild radius. Later in 1931, Abbe Georges Lemaitre proved that the singularity at the Schwarzschild radius was just a coordinate singularity and could be avoided with a different set of coordinates [8]. In 1958, David Finkelstein established that "the Schwarzschild surface at $r = 2m$ is not a singularity but acts as a perfect unidirectional membrane: causal influences can cross it but only in one direction" [9]. In other words, Finkelstein states that the Schwarzschild surface corresponds to the event horizon of static black holes.

In 1963, Roy Kerr published a paper on a new exact solution to Einstein's field equations in a rotating spacetime and presented it in the first Texas Symposium on Relativistic Astrophysics in Dallas, Texas [10], [11]. This was a monumental moment since the observational results can be explained much better with a solution in a rotating spacetime than with a solution in a static spacetime. Today, the black hole occurring in the rotating spacetime is called a Kerr black hole. In 1965, Ezra Newman added the charge concept into the picture created by Kerr and found an exact solution in a charged, rotating spacetime [12], [13]. Today, the metric representing the charged and rotating spacetime is called as the Kerr-Newman metric.

Nevertheless, for years, black holes have been seen as mathematical oddities that only occur at theories. It has been believed that they are too unimaginable to be real, and with a proper correction, they have been expected to vanish from the theory. In 1965, this idea changed. Roger Penrose published a paper and proved that black holes are not just mathematical defects, but they are inevitable in real life [14], [15]. With the help of this paper and observational discoveries occurring at the same time, black hole research became a crucial subject in the field. Although there have been significant developments in the black hole research since then, some essential points remain unsolved. Two such points constitute the main problems investigated in this thesis.

1.2 Outline

One of the strangest properties of black holes is that they can bend the spacetime fabric with their enormous gravity so that they can force a photon to follow an orbit around them. These are called light orbits. These orbits are unstable, so even under a small perturbation, they can spread out to space or fall into the black hole. This makes them extremely important for observational black hole research because they can carry information about the black hole. Therefore, it is crucial to understand these light orbits. Especially, the light orbits with constant radii are astrophysically relevant. Unfortunately, only for few specific cases an exact solution describing the constant radii light orbit in terms of the black hole rotation or spin parameter and the effective inclination angle of the orbit can be found. In Chapter 2, we propose a new family of exact solutions. An efficient approximation is also provided to understand these orbits in other cases with no known exact solutions. In Chapter 3, the method provided in Chapter 2 is extended to cover massive particle orbits. An approximate solution is provided to understand these timelike orbits.

Another interesting property of a black hole is the event horizon. The event horizon is the boundary of the black hole region from which causal geodesics cannot reach future null infinity [16]. The standard way to detect the event horizon depends on the knowledge of the metric of the spacetime in some coordinates. Therefore, this approach is called the coordinate-dependent approach. In other words, the detection of the event horizon depends on the specific set of coordinates assigned to the spacetime. In order to avoid this dependence, a coordinate-independent way has been developed. In this method, the spacetime is characterized by some curvature invariants. With the help of these invariants and their combinations, it is possible to detect the event horizon. In the fourth Chapter, we propose a method to detect the event horizon of black holes with dimensions $D > 2$ in a coordinate-independent way.

1.3 Light Orbits [1]

Observational black hole physics, using gravitational waves or radio waves, is currently thrilling: since the first black hole merger observation via gravitational waves [18], there has been more than a dozen observations, including the most recent groundbreaking detection of a binary black hole system with a total mass of $150\ M_\odot$ [19]. With radio waves, the Event Horizon Telescope provided us with a stunning image of

[1] This part is based on the paper 'Exact formulas for spherical photon orbits around Kerr black holes' written by Aydin Tavlayan and Prof. Dr. Bayram Tekin published by Physical Review D in 2020 [17].

the environment and the shadow of a supermassive black hole [20]. All these black holes are described by the Kerr solution of the vacuum Einstein equation with mass m and angular momentum J [10] and no other parameters. Hence, studying physics, especially the motion of ultrarelativistic particles and light around the Kerr black hole metric, is extremely relevant to the current observations, especially in the context of imaging the black hole and the ring-down phase of a merger.

Among the light orbits around a rotating black hole, there is a particular class with constant radii that are astrophysically relevant [21]. For this class of light orbits, there are exact expressions of their radii in terms of the black hole rotation or spin parameter and the effective inclination angle of the orbit for only two special cases. These are the equatorial orbits (called the light rings) and the polar orbit, but in between these two extremes, called the spherical photon orbits [22], there are no known exact solutions in the literature. Here exact expressions for an important class of such orbits that are not restricted to the equatorial or polar planes are provided. For these orbits, there is a relation between the inclination angle and the black hole rotation parameter. Moreover, this angle turns out to be critical in the sense that there are four null geodesics below it, albeit two of these are inside the event horizon for nonextremal black holes; one of the external orbits has a nonmonotonic dependence on the rotation parameter of the black hole in contrast to the monotonic dependence of the polar and equatorial orbits. On the other hand, above the critical inclination angle, there are only two spherical null geodesics. An approximate analytical expressions not only for the critical case but also for the case of generic inclination angle shall also be given.

1.4 Curvature Invariants [2]

The event horizon of a black hole is a codimension one null hypersurface, which constitutes the boundary of the black hole region from which casual geodesics cannot reach future null infinity [16]. As such, the event horizon is highly non-local in

[2] This part is based on the paper 'Event horizon detecting invariants' written by Aydin Tavlayan and Prof. Dr. Bayram Tekin published by Physical Review D in 2020 [23].

time, and so one a priori needs the full knowledge of the spacetime to locate it. In this respect, for example, the image obtained by the Event Horizon Telescope (EHT) contains the environment of the black hole as well as the codimension two cross-section of the event horizon but not the event horizon which is a 2+1 dimensional hypersurface.

Given a metric representing a spacetime, the usual search for an event horizon proceeds as follows: one assumes that the event horizon $\mathcal{H}$ is a smooth level set of a single function F satisfying $g^{\mu\nu}\partial_\mu F \partial_\nu F = 0$ which clearly requires well-chosen coordinates in spacetime. Instead of this coordinate-dependent method, there have been some recent developments initiated by the work of Abdelqader and Lake [24] who gave an invariant characterization of the Kerr black hole, significantly extending the earlier method of Karlhede *et al.* [25] which works for the case of the Schwarzschild black hole. In [24] the following set of curvature scalars was suggested as a basis to detect the location of the event horizon and the ergosurface as well as to define some other properties, such as the mass and the spin of the black hole

$$\begin{aligned}
&I_1 = C_{\mu\nu\alpha\beta}C^{\mu\nu\alpha\beta}, \qquad I_2 = {}^*C_{\mu\nu\alpha\beta}C^{\mu\nu\alpha\beta}, \\
&I_3 = \nabla_\rho C_{\mu\nu\alpha\beta}\nabla^\rho C^{\mu\nu\alpha\beta}, \quad I_4 = \nabla_\rho C_{\mu\nu\alpha\beta}\nabla^{\rho *} C^{\mu\nu\alpha\beta}, \\
&I_5 = k_\mu k^\mu, \quad I_6 = l_\mu l^\mu, \qquad I_7 = k_\mu l^\mu,
\end{aligned} \tag{1.1}$$

where $C_{\mu\nu\alpha\beta}$ is the Weyl Tensor, ${}^*C_{\mu\nu\alpha\beta}$ is its left dual which is defined as ${}^*C_{\mu\nu\alpha\beta} = \frac{1}{2}\epsilon_{\mu\nu\gamma\delta}C^{\gamma\delta}{}_{\alpha\beta}$ and the two covectors defining the last three scalars are given as $k_\mu = -\nabla_\mu I_1$, and $l_\mu = -\nabla_\mu I_2$. To detect the location of the event horizon of the Schwarzschild black hole I_3 is sufficient: Namely, that scalar is positive outside the event horizon, vanishes on the event horizon, and is negative inside the horizon. For the Kerr black hole, none of the above invariants are enough to locate the event horizon. Hence in [24], the following nonlinear combination was found

$$Q_2 = \frac{1}{27}\frac{I_5 I_6 - I_7^2}{(I_1^2 + I_2^2)^{5/2}}, \tag{1.2}$$

which vanishes on the event horizon of the Kerr black hole. In constructing this invariant, three syzygies that are valid for the Kerr black hole were found among the seven invariants (1.1), reducing the independent invariants to four, which are sufficient to invariantly describe the mass, spin, and the r, θ coordinates of the cohomogeneity of the metric.

As can be deduced from the above discussion, for each kind of black hole, one must judiciously define a curvature scalar that can be used to detect the event horizon. This *ad hoc* state of affairs was remedied by Page and Shoom [26], who proposed a systematic way of constructing such invariants. The crux of their idea boils down to the fact that the event horizon is a null hypersurface with a degenerate metric; as such, the determinant of the hypersurface metric vanishes on the event horizon. However, this statement can be invariantly stated not with the coordinates (which are scalar functions defined on open subsets of the spacetime manifold) but with some other scalar functions built from curvature invariants. The execution of their procedure is as follows: the squared norm of the wedge product of n gradients of independent local smooth curvature invariants would vanish on the horizon of any stationary black hole, where n is the local cohomogeneity of the spacetime.

The Page-Shoom method is powerful, but it does not work for the critical example of the 2+1 dimensional BTZ black hole [27], which is a solution of Einstein's theory with a negative cosmological constant, as well as any other three dimensional gravity theory which admits AdS_3 as a solution. The reason for this failure is simple to understand: in three dimensions, the Riemann tensor is algebraically related to the Einstein tensor as $R_{\mu\alpha\nu\beta} = \epsilon_{\mu\alpha\sigma}\epsilon_{\nu\beta\rho}G^{\sigma\rho}$: hence whenever the Einstein tensor vanishes, the Riemann tensor vanishes along with all the curvature invariants; and whenever the Einstein tensor is proportional to the metric tensor (as in the case of the BTZ black hole) the Riemann tensor is locally maximally symmetric as in AdS_3 and all the curvature invariants are just constants. The conclusion is that the spacetime curvature scalars cannot be used to detect the event horizon of the BTZ black hole. This prompted me to search for a new approach that is described in this work.

CHAPTER 2

EXACT FORMULAS FOR SPHERICAL PHOTON ORBITS AROUND KERR BLACK HOLES

2.1 Null Geodesics

The metric of the Kerr black hole with mass m and angular momentum $J = ma$ in the Boyer-Lindquist coordinates (in the $G = c = 1$ units) is

$$\begin{aligned} ds^2 \;\; = \;\; & -\Big(1 - \frac{2mr}{\Sigma}\Big)dt^2 - \frac{4mar\sin^2\theta}{\Sigma}dtd\phi + \frac{\Sigma}{\Delta}dr^2 \\ & +\Sigma\, d\theta^2 + \Big(r^2 + a^2 + \frac{2ma^2 r\sin^2\theta}{\Sigma}\Big)\sin^2\theta d\varphi^2, \end{aligned} \tag{2.1}$$

where a is called the rotation parameter defined in the range $0 \leq a \leq 1$, and the two functions are given as

$$\Delta \equiv r^2 - 2mr + a^2, \qquad \Sigma \equiv r^2 + a^2\cos^2\theta. \tag{2.2}$$

The larger root of $\Delta = 0$ is the event horizon located at

$$r_{\mathrm{H}} = m + (m^2 - a^2)^{1/2}. \tag{2.3}$$

To solve the geodesic equations for a photon in the Kerr spacetime, four constants of motion are necessary. Two of them are obtained from the symmetries that the spacetime possesses. One of them is the rest mass of the particle. The fourth one was introduced by Carter in 1968 [28], [29]. Four geodesic equations obtained for photon

[22] are

$$\Sigma\frac{\mathrm{d}r}{\mathrm{d}\lambda} = \pm\sqrt{R(r)}, \tag{2.4}$$

$$\Sigma\frac{\mathrm{d}u}{\mathrm{d}\lambda} = \pm\sqrt{V(u)}, \tag{2.5}$$

$$\Sigma\frac{\mathrm{d}\varphi}{\mathrm{d}\lambda} = \frac{L_z}{1-u^2} + \frac{a}{\Delta}(2mrE - aL_z), \tag{2.6}$$

$$\Sigma\frac{\mathrm{d}t}{\mathrm{d}\lambda} = -a^2E\left(1-u^2\right) + \frac{1}{\Delta}\left[E\left(r^2+a^2\right)^2 - 2mraL_z\right], \tag{2.7}$$

where λ is an affine parameter along the null geodesics and

$$R(r) \equiv E^2r^4 + \left[a^2E^2 - \mathcal{Q} - L_z^2\right]r^2 \tag{2.8}$$
$$+2m\left[(aE-L_z)^2 + \mathcal{Q}\right]r - a^2\mathcal{Q},$$

$$V(u) \equiv -a^2E^2u^4 - \left[\mathcal{Q} + L_z^2 - a^2E^2\right]u^2 + \mathcal{Q}, \tag{2.9}$$

$$u \equiv \cos(\theta). \tag{2.10}$$

For the spherical photon orbits, the relevant part of the geodesic equations is the radial one, (2.4). Here E is the conserved energy of the photons (related with the $\xi_{(t)} = \frac{\partial}{\partial t}$ Killing vector of the metric), L_z is the conserved z-component of the angular momentum of the photons (related to the $\xi_{(\varphi)} = \frac{\partial}{\partial\varphi}$ Killing vector), and $\mathcal{Q}$ is the Carter's constant related with a symmetric rank two Killing tensor whose explicit form is not needed here; it suffices to know that it is connected with the motion perpendicular to the equatorial plane and $\mathcal{Q} \geq 0$ for constant radii orbits, satisfying the bound for equatorial orbits.

Two equations must be satisfied, $R(r) = 0$ and $\frac{dR(r)}{dr} = 0$, for constant radius r null geodesics. These yield the following (physically viable) equations [22]:

$$\frac{L_z}{E} = -\frac{r^3 - 3mr^2 + a^2r + a^2m}{a(r-m)}, \tag{2.11}$$

$$\frac{\mathcal{Q}}{E^2} = -\frac{r^3\left(r^3 - 6mr^2 + 9m^2r - 4a^2m\right)}{a^2(r-m)^2}. \tag{2.12}$$

Defining the *effective inclination angle* as [30]

$$\cos i \equiv \frac{L_z}{\sqrt{L_z^2 + \mathcal{Q}}}, \tag{2.13}$$

which is clearly a conserved quantity, and noting the fact that photons with different energies can orbit at the same radius as dictated by the equivalence principle, one can eliminate the energy of the photon in (2.11, 2.12). To achieve that, first, the variables in these equations are made dimenisonless by the following definitions

$$x \equiv \frac{r}{m}, \qquad u \equiv \frac{a^2}{m^2}, \qquad \nu \equiv \sin^2 i. \tag{2.14}$$

Then, by combining (2.11) and (2.12), the following sextic polynomial equation is obtained [See Appendix A for the derivation]

$$\begin{aligned} p(x) \;\equiv\; & x^6 - 6x^5 + (9 + 2\nu u)x^4 - 4ux^3 \\ & -\nu u(6-u)x^2 + 2\nu u^2 x + \nu u^2 = 0. \end{aligned} \tag{2.15}$$

From now on, we will call u to be the rotation parameter. So, one must solve this polynomial equation as $x = x(u, \nu)$ for the following intervals to obtain information about the motion of the photon:

$$0 < x, \qquad 0 \leq \nu \leq 1, \qquad 0 \leq u \leq 1. \tag{2.16}$$

Let us first briefly discuss the known solutions in the particular cases before presenting novel solutions.

2.2 Equatorial and Polar Orbits

To study the equatorial orbits ($\mathcal{Q} \equiv 0$) , let $i = 0$ or π. Then $\nu = 0$ and the nontrivial part of the sextic (2.15) reduces to the cubic

$$x^3 - 6x^2 + 9x - 4u = 0. \tag{2.17}$$

For $u = 1$, which is the extremal black hole case, there is a double root at $x = 1$ and another root at $x = 4$. The double root has the same r-coordinate as the event horizon, but they are not located at the same point as the horizon due to the extended geometry of the extremal black hole's throat. This tricky case was addressed in [31, 32]. For the subextremal case, $u < 1$, there are three distinct real roots,

$$x_\pm = 2 + 2\cos\left(\frac{2}{3}\cos^{-1}(\pm\sqrt{u})\right), \tag{2.18}$$

$$x_{\text{in}} = 4\sin^2\left(\frac{1}{3}\sin^{-1}\sqrt{u}\right), \tag{2.19}$$

where x_+ is the retrograde orbit satisfying $3 \leq x_+ \leq 4$, while x_- is the prograde orbit satisfying $1 \leq x_- \leq 3$. The third orbit is inside the event horizon: $0 < x_{\text{in}} \leq 1$. In figure (2.1), the real roots of the sextic polynomial equation on the equatorial plane are plotted as a function of the rotation paramater.

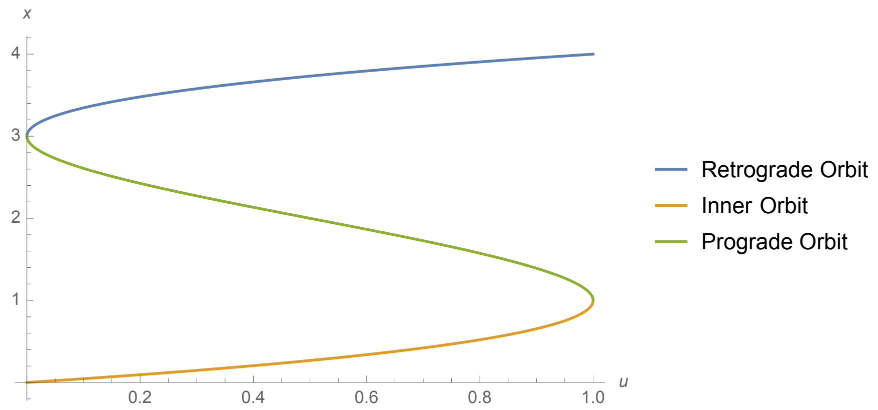

Figure 2.1: Real roots of the sextic polynomial are plotted as a function of the rotation parameter on the equatorial plane.

For the polar orbit ($L_z = 0$), and so $i = \pm\frac{\pi}{2}$, then $\nu = 1$ and (2.15) reduces to

$$x^3 - 3x^2 + ux + u = 0. \tag{2.20}$$

There are three real solutions, but one of the solutions has $x < 0$ and hence it is unphysical. The external solution is

$$x_P = 1 + 2\sqrt{1 - \frac{u}{3}} \cos\left\{\frac{1}{3}\cos^{-1}\left(\frac{1-u}{\left(1-\frac{u}{3}\right)^{3/2}}\right)\right\}, \tag{2.21}$$

which lies in the region $1 \leq x_P \leq 3$. The interior solution is

$$x_{\text{in}} = 1 - 2\sqrt{1 - \frac{u}{3}} \sin\left\{\frac{1}{3}\sin^{-1}\left(\frac{1-u}{\left(1-\frac{u}{3}\right)^{3/2}}\right)\right\}, \tag{2.22}$$

which lies in the region $0 < x_{\text{in}} \leq 1$. The photons in these polar orbits have zero angular momentum, but they do rotate with the black hole as a result of the frame-dragging (or the Lense-Thirring) effect. In figure (2.2), the real roots of the sextic polynomial equation on the polar plane are plotted as a function of the rotation paramater.

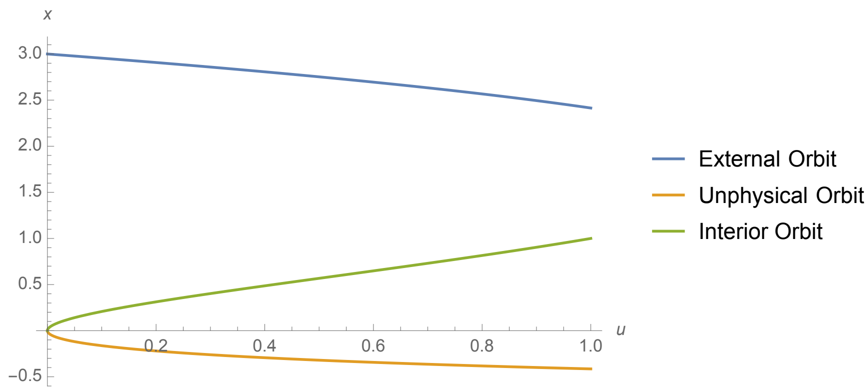

Figure 2.2: Real roots of the sextic polynomial are plotted as a function of the rotation parameter on the polar plane.

2.3 Schwarzschild Black Hole

For $u = 0$, the case for which the Kerr black hole has no rotation and reduces to the Schwarzschild black hole, the nontrivial part of (2.15) for generic ν simplifies to

$$x - 3 = 0, \tag{2.23}$$

which is the radius of the circular photon ring (or the light ring) independent of the inclination angle due to the spherical symmetry.

2.4 Spherical Photon Orbits

For generic ν and u, there are four sign variations in the polynomial (2.15), (+, -, +, -, -, +, +), and hence Descartes' rule of sign change says that there can be 4, 2, or 0 positive roots. Using a Tschirnhaus transformation of the form $y = \alpha x^4 + \beta x^3 + \gamma x^2 + \delta x + \epsilon$, the sextic can be brought to the reduced form $y^6 + c_1 y^2 + c_2 y + c_3 = 0$, albeit with very complicated coefficients $c_i = c_i(u, \nu)$. The exact expressions of the roots in the generic case of any polynomial beyond the quartic, in terms of a finite number of radicals, are not possible as dictated by the celebrated Abel-Ruffini impossibility theorem [See Appendix B for the statement of this theorem]. This theorem applies to the sextic in the original or reduced form. However, one can certainly find exact formulas for the roots in terms of special functions such as the Mellin formula [33], theta functions [34], or the nested radicals [See Appendix C for nested radicals]. Because of the complexity of exact roots in the most general form, let us concentrate on particular values of ν and u of the sextic for which exact solutions in radicals can be found. Remarkably, this will turn out to be possible.

As the real roots of the sextic are being searched for, the point in the (u, ν) parameter space where four real and two complex roots arise as allowed by the Descartes' rule of sign might be found. It turns out for a given rotation parameter u, there is a *critical inclination angle* below which there are four real roots and above which there are two real roots. For this critical value, $\nu_{\text{cr}} = \nu_{\text{cr}}(u)$, the discriminant of the sextic vanishes [See Appendix D for more information about the discriminant of a polynomial], and one can find all the roots of the sextic in an exact form.

To proceed further, it pays to define the following variables which will simplify the final expressions:

$$\nu \equiv \frac{\xi}{u}, \qquad u \equiv 1 - w^3, \tag{2.24}$$

with $0 \leq \xi \leq 1$ and $0 \leq w \leq 1$. Then it can be shown that the sextic (2.15) reduces to a quadratic times a quartic at the following critical point:

$$\xi_{\text{cr}} = \frac{3(1-w)^3}{7 + (w-5)w}. \tag{2.25}$$

[See Appendix E for the detailed derivation of the critical angle]. The domain of ξ_{cr} is $[0, \frac{3}{7}]$. Note that previously in [35], one particular point in this critical domain was discovered: namely, it was shown that the critical angle corresponding to the extremal black hole ($u = 1$) is $\cos i = \sqrt{4/7}$ or $\nu = \frac{3}{7}$. Here with the formula (2.25) the critical angle for *any* rotating parameter is given. So, at this critical angle, the sextic factors as

$$p(x) = (w + x - 1)^2 q(x), \tag{2.26}$$

with the quartic part given as

$$q(x) = x^4 + \alpha x^3 + \beta x^2 + \gamma x + \sigma, \tag{2.27}$$

where the coefficients are

$$\begin{aligned}
\alpha &= -2(w+2), \\
\beta &= \frac{3w\Big(w^2(w-5)+3w+8\Big)+6}{(w-5)w+7}, \\
\gamma &= \frac{6(w-2)(w-1)\left(w^2+w+1\right)}{(w-5)w+7}, \\
\sigma &= \frac{3(w-1)^2\left(w^2+w+1\right)}{(w-5)w+7}.
\end{aligned} \tag{2.28}$$

The quadratic part has a double root at

$$x = 1-(1-u)^{\frac{1}{3}} \tag{2.29}$$

inside the event horizon for finite u and approaches the event horizon as $u \to 1$. The quartic part has generically two real and two complex roots, which can be written in explicit form, but the expressions are rather cumbersome, and so is not depicted here. These explicit formulas can be used, with the help of a computer, to understand the properties of the orbits exactly. Here several such computations are given.

In figure (2.3), the real roots of the sextic polynomial equation as a function of the rotation parameter at the critical inclination angle are plotted. One can see how the roots are connected with each other and observe the nonmonotonic behavior of the retrograde orbit. Note that, as opposed to the critical retrograde orbit, shown in figure (2.3), the equatorial retrograde orbit, shown in figure (2.1) is monotonic in the rotation parameter; all the other roots are also monotonic. In the figure (2.4), the dimensionless angular momentum per energy, $\frac{L_z}{mE}$, as given in (2.11) is plotted as a function of rotation parameter. In Fig. (2.5), $\frac{d^2R}{dx^2}$ is plotted as a function of rotation parameter and it is shown that the critical null geodesics are unstable in the radial direction as expected: all spherical photon orbits are unstable in the radial direction. This fact makes them very interesting as they can escape to infinity even with a small perturbation, and this is part of the light detected by the Event Horizon Telescope. In Fig. (2.6), the dimensionless impact parameter for the retrograde orbits at the critical inclination angle and at the equator is plotted. Among all the orbits, the retrograde orbit has the highest impact parameter. Figure (2.7) shows the analogous plot for the prograde orbits.

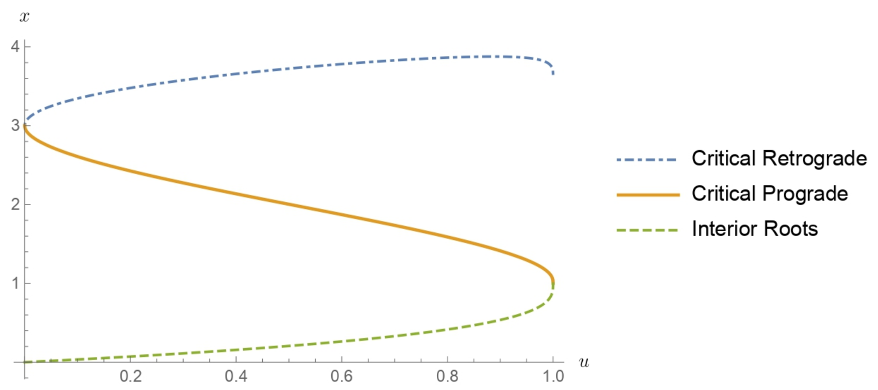

Figure 2.3: Real roots of the sextic are plotted as a function of the rotation parameter at the critical inclination angle. The root corresponding to the retrograde orbit is nonmonotonic in u while the other roots are monotonic. Note that the third and the fourth roots are double roots and lie inside the event horizon for the nonextremal black hole.

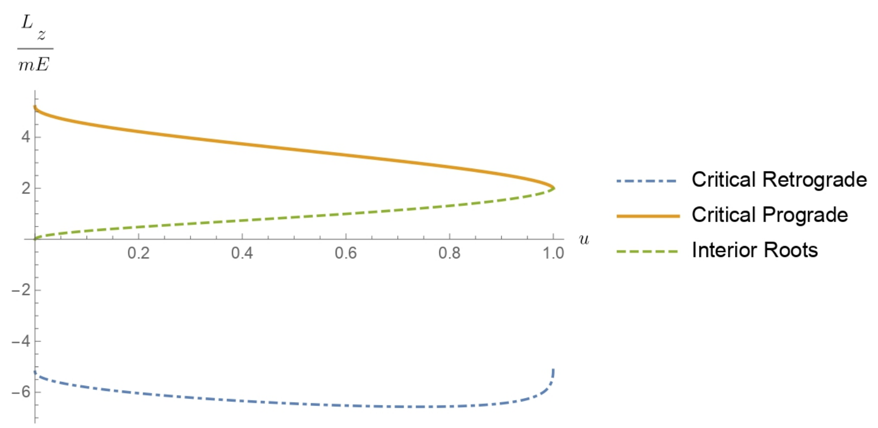

Figure 2.4: The z-component of the angular momentum per unit energy and black hole mass is plotted for the real roots at the critical point as a function of the rotation parameter. The root corresponding to the retrograde orbit with a negative angular momentum component has a nonmonotonic dependence on u.

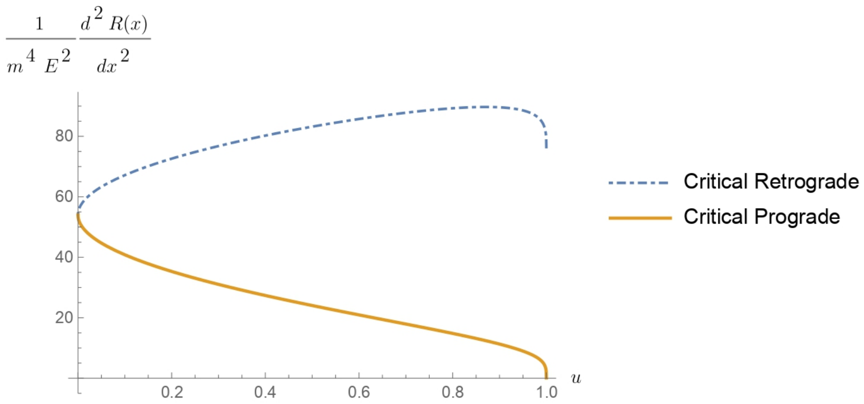

Figure 2.5: Second derivative of R from (2.8) is given for the critical photon orbits: for the exterior roots, the second derivative is positive and hence they are unstable orbits just like the prograde, retrograde, and the polar orbits. For the interior double root, the second derivative vanishes, so that root is a saddle point.

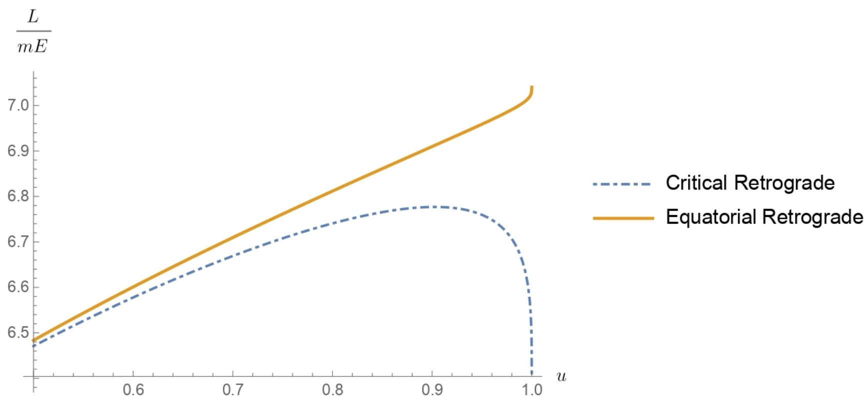

Figure 2.6: The dimensionless "impact parameter" $\frac{L}{mE}$ with $L = \sqrt{L_z^2 + \mathcal{Q}}$ for the retrograde orbits at the critical inclination angle and at the equatorial plane are plotted. The equatorial retrograde orbit has the highest impact parameter and is monotonic in the rotation parameter, while the impact parameter of the critical retrograde orbit is nonmonotonic.

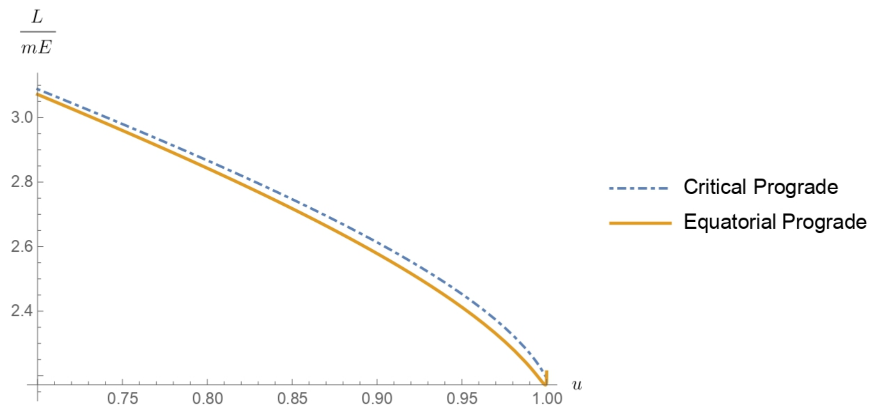

Figure 2.7: The dimensionless "impact parameter" for the critical and equatorial prograde orbits are nonmonotonic in the impact parameter and they are both smaller than those of retrograde orbits.

2.5 Approximate Solutions

Here, a method to determine approximate solutions around any of the known solutions presented above is developed. This method is based on the Lagrange-Bürmann inversion theorem [36] [See Appendix F for the statement of the theorem]. Let us assume f to be a function of the form

$$f(x) = \nu, \qquad \frac{df(x)}{dx}\Big|_{x=x_0} \neq 0. \tag{2.30}$$

Then the Lagrange-Bürmann inversion theorem states that one can write x as a power series in ν of the form

$$x = x_0 + \sum_{n>0} \frac{g_n}{n!}\Big(\nu - f(x_0)\Big)^n, \tag{2.31}$$

where

$$g_n = \lim_{x\to x_0} \frac{d^{n-1}}{dx^{n-1}}\left(\frac{x-x_0}{f(x)-f(x_0)}\right)^n, \quad n = 1, 2, \dots\,. \tag{2.32}$$

To apply this method to the sextic polynomial equation, for a given u, one can solve for ν in (2.15) to get the inclination angle as a function of the radius as

$$\nu(x) = -\frac{x^3\Big((x-3)^2x - 4u\Big)}{u\Big(u(x+1)^2 + 2\left(x^2-3\right)x^2\Big)}. \tag{2.33}$$

For x_0, as stated above, one can choose any of the known solutions. Here, for the sake of simplicity, let us choose the prograde and the retrograde orbits on the equatorial plane, (2.18), as examples. Then $x_0 = x_\pm$ and $\nu(x_0) = 0$; one can easily compute the approximate solution up to the desired order. Here an approximate solution up to $\mathcal{O}(\nu)$ shall be presented as it already yields an accurate approximation. Then, from (2.32), one finds

$$g_1 = \lim_{x \to x_0} \left(\frac{x - x_0}{\nu} \right),$$

which yields

$$\begin{aligned} g_1 &= \frac{A(x_0)}{B(x_0)}, \\ A(x_0) &= u\Big(u(x_0+1)^2 + 2x_0^4 - 6x_0^2\Big)^2 \\ B(x_0) &= 4x_0^2(x_0+3)\Big(u(x_0+1) + x_0^3 - 3x_0^2\Big) \\ &\quad \times \Big(u - x_0^3 + 3x_0^2 - 3x_0)\Big). \end{aligned} \tag{2.34}$$

Then, the resulting approximate solution is

$$x = x_0 + g_1\nu + \mathcal{O}(\nu^2), \tag{2.35}$$

which is accurate for small $\nu \approx 0.1$ by two parts in 10^4 for slowly rotating black holes, $u \approx 0.1$, and by two parts in 10^3 for fast rotating ones, $u \approx 0.9$, around the prograde equatorial orbits. The approximation works better for retrograde orbits.

For better accuracy, one needs to compute higher-order terms. Some examples up to and including $\mathcal{O}(\nu^4)$ is shown in the tables. As errors show, the approximation is exceptionally accurate. In Table I and II, the exact numerical values are compared with the approximate analytical ones obtained via the Lagrange-Bürmann expansion, respectively, around the prograde and retrograde orbits at the equatorial plane. Near $\nu = 0$, around which the series was expanded, the error is less than one part in 10^4 for all of the rotation parameter values. The error becomes larger for larger values of ν: for example, for $\nu = 0.5$, the error is 0.24% for highly spinning black holes. Hence, one can use these approximate analytical formulas to explore the behavior of these orbits.

Table 2.1: Comparison of approximate and exact numerical results around the prograde orbit at the equator, $x_0 = x_+$. Approximation is done with the Lagrange-Bürmann expansion up to order $\mathcal{O}(\nu^5)$.

ν	u	$x_{\text{approximate}}$	x_{exact}	Error (%)
0.1	0.1	2.6247277	2.6247278	4.3×10^{-6}
0.1	0.5	2.027428	2.027429	1.4×10^{-5}
0.1	0.9	1.411893	1.411895	7.5×10^{-5}
0.5	0.1	2.7033	2.7038	1.9×10^{-2}
0.5	0.5	2.174	2.175	6×10^{-2}
0.5	0.9	1.562	1.565	2.4×10^{-1}

Table 2.2: Comparison of approximate and exact numerical results around the retrograde orbit at the equator, $x_0 = x_-$. Approximation is done with the Lagrange-Bürmann expansion up to order $\mathcal{O}(\nu^5)$.

ν	u	$x_{\text{approximate}}$	x_{exact}	Error (%)
0.1	0.1	3.3249272	3.3249271	3.3×10^{-6}
0.1	0.5	3.6801618	3.6801615	7.6×10^{-6}
0.1	0.9	3.8803947	3.8803943	1.1×10^{-5}
0.5	0.1	3.228	3.227	1.6×10^{-2}
0.5	0.5	3.438	3.437	3.8×10^{-2}
0.5	0.9	3.533	3.531	5.6×10^{-2}

CHAPTER 3

SPHERICAL GEODESICS FOR MASSIVE PARTICLES

3.1 Timelike Geodesics

In the standard Boyer-Lindquist coordinates (t, r, θ, ϕ), the Kerr metric can be written as

$$\begin{aligned} ds^2 \quad = \quad & -\left(1 - \frac{2Mr}{\Sigma}\right) dt^2 - \frac{4Mr}{\Sigma} a \sin^2\theta dt d\phi + \Sigma\left(\frac{dr^2}{\Delta} + d\theta^2\right) \\ & + \left(r^2 + a^2 + \frac{2Mr}{\Sigma} a^2 \sin^2\theta\right) \sin^2\theta d\phi^2, \end{aligned} \tag{3.1}$$

where

$$\begin{aligned} \Sigma &= r^2 + a^2\cos^2\theta, \\ \Delta &= r^2 - 2Mr + a^2. \end{aligned} \tag{3.2}$$

The four geodesic equations governing the motion of a particle with mass μ are

$$\begin{aligned} \Sigma\frac{dr}{d\tau} &= \pm\sqrt{R(r)}, \\ \Sigma\frac{d\cos\theta}{d\tau} &= \pm\sqrt{V(\cos\theta)}, \\ \Sigma\frac{d\phi}{d\tau} &= \frac{L_z}{1-\cos^2\theta} + \frac{a}{\Delta}\left(2MrE - aL_z\right), \\ \Sigma\frac{dt}{d\tau} &= -a^2E\left(1-\cos^2\theta\right) + \frac{1}{\Delta}\left(E\left(r^2+a^2\right)^2 - 2MraL_z\right), \end{aligned} \tag{3.3}$$

where

$$\begin{aligned} R(r) = \quad & r^2\left(a^2\left(E^2-\mu^2\right) - Q - L_z^2\right) - a^2Q + 2Mr\left((aE-L_z)^2 + Q\right) \\ & + r^4\left(E^2-\mu^2\right) + 2\mu^2Mr^3 \end{aligned} \tag{3.4}$$

and,

$$V(\cos\theta) = a^2\left(\mu^2 - E^2\right)\cos^4\theta - \left(a^2\left(\mu^2 - E^2\right) + Q + L_z^2\right)\cos^2\theta + Q. \quad (3.5)$$

Here, τ is an affine parameter along the geodesic. E, L_z and Q are constants of motion which correspond to the energy of the particle, the z-component of the angular momentum of the particle and the Carter's constant, respectively. In order to simplify the following calculations, let us rescale as

$$r = Mx, \quad a = M\tilde{a}, \quad Q = M^2\mu^2\tilde{Q}, \qquad L_z = M\mu\tilde{L}_z, \quad E = \mu\tilde{E}, \quad (3.6)$$

which removes the mass (M,μ) dependence of the radial geodesic equation to arrive at

$$\frac{R(r)}{\mu^2 M^4} = x^2\left(\tilde{a}^2\left(\tilde{E}^2 - 1\right) - \tilde{Q} - \tilde{L}_z^2\right) - \tilde{a}^2\tilde{Q} + 2x\left((\tilde{a}\tilde{E} - \tilde{L}_z)^2 + \tilde{Q}\right) + x^4\left(\tilde{E}^2 - 1\right) + 2x^3. \quad (3.7)$$

By defining the obviously conserved *effective inclination angle* as

$$\cos i \equiv \frac{L_z}{\sqrt{L_z^2 + \mathcal{Q}}}, \quad (3.8)$$

and

$$\nu = \sin^2 i, \quad (3.9)$$

the Carter's constant can be put into the form

$$Q = \frac{\nu L_z^2}{1-\nu}. \quad (3.10)$$

Using the last equation in the conditions for spherical geodesics

$$R(r) = 0, \quad \frac{dR}{dr} = 0, \quad (3.11)$$

and with the help of the redefinitons

$$u = \tilde{a}^2, \quad k = \tilde{E}^2, \quad (3.12)$$

the Carter's constant and the z-component of the angular momentum of the particle can be eliminated and the following polynomial equation can be obtained

$$
\begin{aligned}
p(x) \;=\;& x^{10}\left(k^2-2k+1\right) \\
+\;& x^9\left(-6k^2+14k-8\right) \\
+\;& x^8\left(4\left(k-1\right)^2\nu u+9k^2-32k+24\right) \\
+\;& x^7\left(-2\left(k-1\right)u\left(k(6\nu+2)-11\nu-1\right)+24k-32\right) \\
+\;& x^6\left(4k^2\nu^2u^2-8k\nu^2u^2+2k^2\nu u^2-4k\nu u^2\right. \\
& \quad \left.+2u\left(6k^2\nu-k(23\nu+5)+20\nu+4\right)+4\nu^2u^2+2\nu u^2+16\right) \\
+\;& x^5\left(12k\nu^2u^2-12k^2\nu u^2+24k\nu u^2+16k\nu u-12\nu^2u^2-12\nu u^2\right. \\
& \quad \left.-24\nu u-8u\right) \\
+\;& x^4\left(4k^2\nu^2u^3-12k^2\nu^2u^2-8k\nu^2u^3+12k\nu^2u^2+10k^2\nu u^2\right. \\
& \quad \left.-28k\nu u^2+4\nu^2u^3+9\nu^2u^2+14\nu u^2+u^2\right) \\
+\;& x^3\left(4k^2\nu^2u^3+2k\nu^2u^3-16k\nu^2u^2-4k^2\nu u^3+6k\nu u^3\right. \\
& \quad \left.+8k\nu u^2-6\nu^2u^3-2\nu u^3\right) \\
+\;& x^2\left(k^2\nu^2u^4-4k^2\nu^2u^3-2k\nu^2u^4+10k\nu^2u^3-2k\nu u^3+\nu^2u^4\right) \\
+\;& x\left(2k^2\nu^2u^4-2k\nu^2u^4\right) \\
+\;& k^2\nu^2u^4=0.
\end{aligned} \tag{3.13}
$$

Ideally one would like to find all viable real roots of the form $x = x(k, \nu, u)$, but since it is an order 10 polynomial in x, it cannot be solved analtically in terms of finite number of radicals as stated in the Abel-Ruffini theorem. Therefore, in this thesis, some specific cases with important consequences are investigated.

3.2 The Schwarzschild Limit

The simplest case to start with is the Schwarzschild limit where the rotation parameter is set to zero, $u = 0$. The polynomial simplifies to

$$p(x) = x^6\left(kx^2-3kx-x^2+4x-4\right)^2. \tag{3.14}$$

Nontrivial roots of the polynomial are

$$x_1(k) = \frac{-3k + \sqrt{9k^2 - 8k} + 4}{2 - 2k}, \tag{3.15}$$

$$x_2(k) = \frac{8}{-3k + \sqrt{9k^2 - 8k} + 4}. \tag{3.16}$$

$x_1(k)$ represents solutions that are positive only for a small energy range, $\frac{8}{9} \leq k < 1$ and negative otherwise. On the other hand $x_2(k)$ represents solutions outside the event horizon for particles with energy $\frac{8}{9} \leq k$. When the discriminant of the polynomial (3.13) with respect to x is investigated, it vanishes at $k = 0$ and $k = \frac{8}{9}$. Although we can find solutions outside the event horizon for values $k > \frac{8}{9}$, there is no real solution in the interval $0 < k < \frac{8}{9}$, or in the original variables $0 < E^2 < \frac{8}{9}\mu^2$.

3.3 Zero Energy Solution

Let us consider the zero energy case, $k = 0$. In [37], it was shown that it is possible to have massive particles with zero energy in the ergoregion of a black hole. Hence, with the $k = 0$ condition, (3.13) simplifies to give

$$p(x) = x^2 \left(\nu u^2 + 2\nu u x^2 - 3\nu u x - ux + x^4 - 4x^3 + 4x^2\right)^2. \tag{3.17}$$

This equation implies that there are four orbits, one of which is located outside the event horizon as shown in figure (3.1). In figures (3.2) and (3.3), the exterior root and the event horizon are plotted as functions of rotation parameter, u, at different inclination angle values. It is important to state that at small inclination angle, ν, such as $\nu = 0.2$ as shown in figure (3.2) the exterior root has a monotonic behaviour but at large inclination angle values such as $\nu = 0.8$ as shown in figure (3.3) the exterior root has a non-monotonic behaviour.

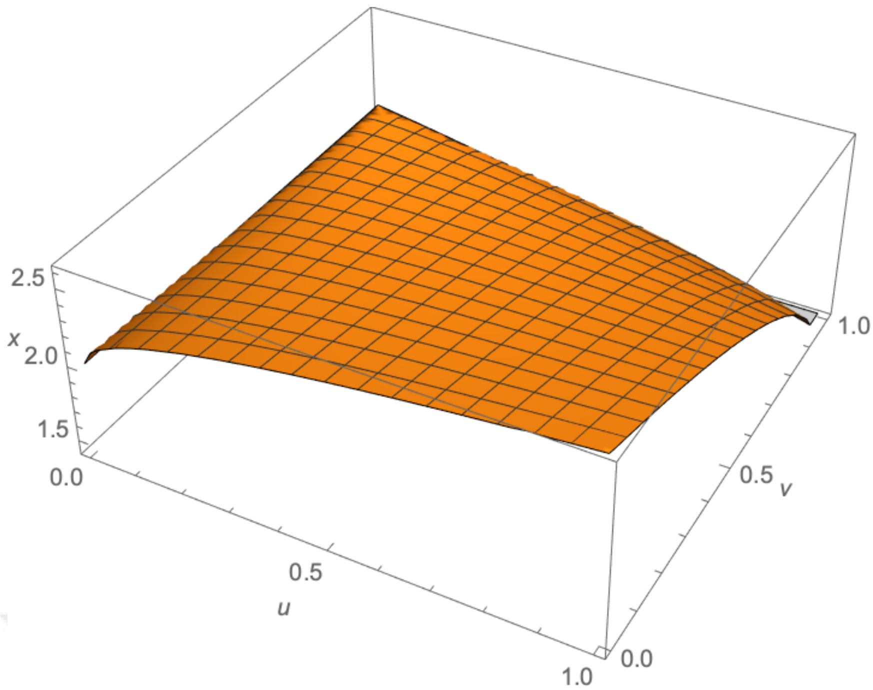

Figure 3.1: Behavior of the orbit of a particle with zero energy outside the event horizon for different rotation parameter, u, and inclination angle, ν, values.

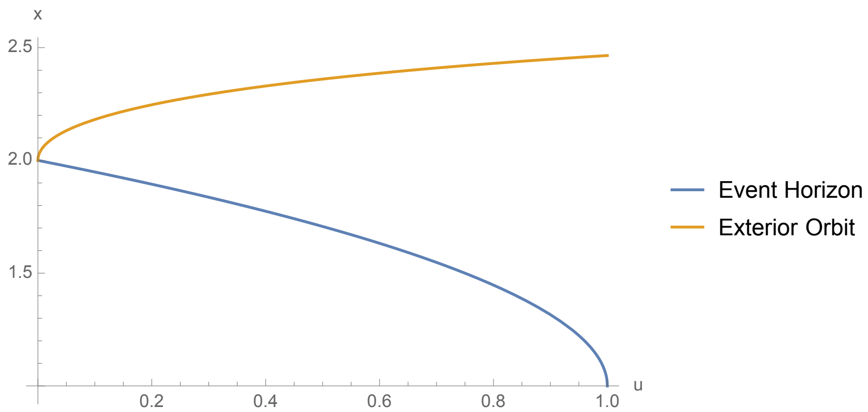

Figure 3.2: The exterior orbit and the event horizon are plotted as a function of rotation parameter, u, at the $\nu = 0.2$ plane.

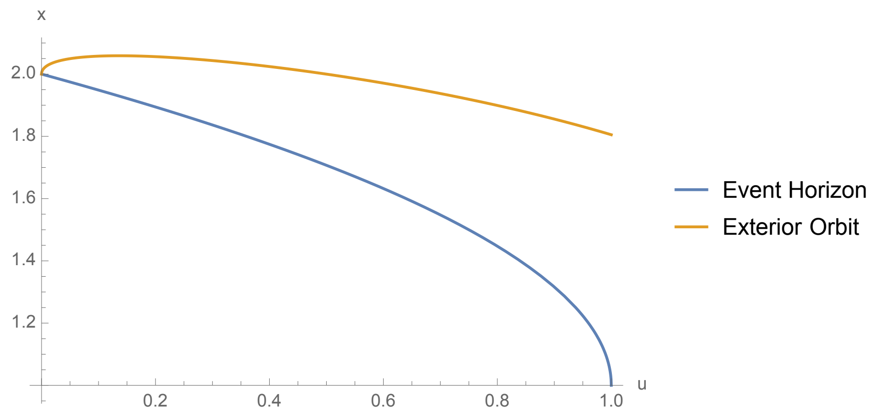

Figure 3.3: The exterior orbit and the event horizon are plotted as a function of rotation parameter, u, at the $\nu = 0.8$ plane.

In order to understand this non-monotonic behaviour, the discriminant of the nontrivial part of the polynomial with respect to rotation parameter should be investigated. The resulting equation becomes

$$\mathcal{D} = 4\nu^2 x^4 - 12\nu^2 x^3 + 9\nu^2 x^2 - 4\nu x^4 + 12\nu x^3 - 10\nu x^2 + x^2. \tag{3.18}$$

At this point, specific x values as function of ν such that $x = x(\nu)$, which make the discriminant, $\mathcal{D}$, vanishes, can be calculated

$$x_1(\nu) = \frac{3}{2} + \frac{1}{2\sqrt{\nu}}, \tag{3.19}$$

$$x_2(\nu) = \frac{3}{2} - \frac{1}{2\sqrt{\nu}}. \tag{3.20}$$

The solution $x_1(\nu)$ provides values outside of the event horizon for the physically viable range of the inclination angle. When the function $x_1(\nu)$ is evaluated at $\nu = 0.8$, it will provide the maximum value of the $x_{\text{max}} = 2.05902$, in other words, the farthest point to where the exterior orbit of the zero energy particle can reach. In order to calculate the corresponding rotation parameter at the maximum point, the polynomial equation should be recalculated with $x = x_1(\nu)$. Specific u value which makes the resulting polynomial equation vanish is

$$u_1 = u_1(\nu) = \frac{\nu\,(2 - 3\sqrt{\nu}) + \sqrt{\nu}}{4\nu^2}. \tag{3.21}$$

$u_1(\nu)$ provides the turning point of x and it can be called the critical rotation parameter. When it is evaluated at $\nu = 0.8$, the result becomes $u = 0.13586$. This result can also be observed in figure (3.3). When $u_1(\nu)$ is evaluated at $\nu = 0.2$, the result becomes $u = 3.61803$. This result is out of the physically meaningful range and that is why a non-monotonicty is not observed in figure (3.2).

3.4 Non-Monotonic Behaviour at Nonzero Energy Values

The non-monotonic behaviour observed for the zero energy particle solution at large inclination angle values in the previous section, can also be observed for particles with positive energy values. Three exemplery cases are shown in the table (3.1). In order to detect the turning point at which non-monotonic behaviour starts, a similar prodecure followed for zero energy particle in the previous section can be followed. First, the discriminant of the polynomial equation (3.13) with respect to the rotation parameter, u, is calculated:

$$\begin{aligned}\mathcal{D} \;=\; & 256k^2(\nu-1)^2\nu^2x^{18}(kx-x+1)^2 \\ & \times(3k\nu x+kx+4\nu-3\nu x-x)^2 \\ & \times\left(-4k\nu+k\nu x^2-kx^2-\nu x^2+x^2+2\nu x-2x\right)^2 \\ & \times\left(256k^2\nu^2+16k^4\nu^2x^6-64k^3\nu^2x^6+96k^2\nu^2x^6+96k^3\nu^2x^5\right. \\ & \quad -288k^2\nu^2x^5-96k^4\nu^2x^4+288k^3\nu^2x^4-72k^2\nu^2x^4-416k^3\nu^2x^3 \\ & \quad +832k^2\nu^2x^3+144k^4\nu^2x^2-288k^3\nu^2x^2-456k^2\nu^2x^2-64k^4\nu x^4 \\ & \quad +192k^3\nu x^4-200k^2\nu x^4-192k^3\nu x^3+384k^2\nu x^3-168k^2\nu x^2 \\ & \quad +384k^3\nu^2x-384k^2\nu^2x-64k\nu^2x^6+288k\nu^2x^5-336k\nu^2x^4 \\ & \quad -200k\nu^2x^3+600k\nu^2x^2+80k\nu x^4-216k\nu x^3+168k\nu x^2 \\ & \quad -288k\nu^2x-32k\nu x+16\nu^2x^6-96\nu^2x^5+216\nu^2x^4-216\nu^2x^3 \\ & \quad \left.+81\nu^2x^2-8\nu x^4+24\nu x^3-18\nu x^2+x^2\right).\end{aligned} \tag{3.22}$$

Then, non-trivial ν values which make the discriminant, $\mathcal{D}$, vanish are calculated. The physically meaningful result is

$$\nu_{\text{critical}} = \frac{x^2}{A+B} \tag{3.23}$$

where

$$
\begin{aligned}
A \equiv\ & x\left(4\left((k-1)^2(8(k-1)k+1)x^3+3(k-1)(8(k-1)k+1)x^2\right.\right. && (3.24)\\
& \left.\left.+21(k-1)kx+4k\right)+9x\right),
\end{aligned}
$$

and

$$B \equiv -8\sqrt{(1-2k)^2k(2(k-1)x+3)^2\left((k-1)x^2+x\right)^3}. \tag{3.25}$$

At this moment, the turning point can be decided with the help of ν_{critical} and the polynomial equation. For unit energy particles, $k = 1$, the critical inclination angle becomes

$$\nu_{\text{critical}} = \frac{x^2}{x(9x+16)-24\sqrt{x^3}}. \tag{3.26}$$

The x values which make $\nu_{\text{critical}} = 0.9$, as in the table, are $x = 0.973493$ and $x = 4.22548$. The second x value represents a point outside the event horizon and it corresponds to the point at which the maximum of the retrograde orbit occurs. In other words, this is the farthest point a retrograde orbit for unit energy particles at the inclination angle 0.9 can reach. The corresponding rotation parameter value can be calculated with the help of the polynomial equation and it is $u = 0.509021$. The result is consistent with table (3.1).

Three important observations can be made by investigating the table. Firstly, this non-monotonic behaviour can only be observed at large inclination values. Secondly, the threshold inclination angle value decreases for higher energy values. Thirdly, the turning point for rotation parameter decreases for higher energy and higher inclination angle values. In other words, The retrograde orbit starts to retreat at lower u values for higher k and ν values.

Table 3.1: The prograde and retrograde orbits for different energy, k, inclination angle, ν, and rotation parameter, u, values.

k	ν	u	x_{prograde}	$x_{\text{retrograde}}$
1	0.9	0.1	3.74854	4.15469
1	0.9	0.2	3.60934	4.19326
1	0.9	0.3	3.48475	4.21283
1	0.9	0.4	3.36502	4.22241
1	0.9	0.5	3.2458	4.22546
1	0.9	0.6	3.1241	4.22368
1	0.9	0.7	2.99709	4.21809
1	0.9	0.8	2.86137	4.2093
1	0.9	0.9	2.71186	4.19774
2	0.8	0.1	3.00717	3.38174
2	0.8	0.2	2.88105	3.42079
2	0.8	0.3	2.76773	3.44253
2	0.8	0.4	2.65803	3.45524
2	0.8	0.5	2.54757	3.46209
2	0.8	0.6	2.43293	3.46466
2	0.8	0.7	2.31031	3.46387
2	0.8	0.8	2.17403	3.46032
2	0.8	0.9	2.01281	3.45437

3.5 The Unit Energy Situation

Another case which is important to investigate is the unit energy, $k = 1$, case. The polynomial (3.13) turns into

$$\begin{aligned} p(x) \; = \; & x^8 - 8x^7 + x^6(2(3\nu - 1)u + 16) - x^5(8\nu u + 8u) \\ & + x^4 \left(9\nu^2 u^2 - 4\nu u^2 + u^2\right) + x^3 \left(8\nu u^2 - 16\nu^2 u^2\right) \\ & + x^2 \left(6\nu^2 u^3 - 2\nu u^3\right) + \nu^2 u^4. \end{aligned} \tag{3.27}$$

The roots of this polynomial cannot be solved analytically in terms of finite number of radicals. Therefore, auxiliary conditions are required to make it analytically solvable.

3.5.1 Equatorial Plane Solutions

On the equatorial plane

$$\nu = 0, \tag{3.28}$$

at which the polynomial can be written in the form

$$p(x) = p_1(x) \times p_2(x) \tag{3.29}$$

where

$$p_1(x) = x^4, \tag{3.30}$$

and

$$p_2(x) = x^4 - 8x^3 + x^2\,(16 - 2u) - 8ux + u^2, \tag{3.31}$$

of which the roots are

$$x_1(u) = -\sqrt{u} - 2\sqrt{1 - \sqrt{u}} + 2, \tag{3.32}$$

$$x_2(u) = -\sqrt{u} + 2\sqrt{1 - \sqrt{u}} + 2, \tag{3.33}$$

$$x_3(u) = \sqrt{u} - 2\sqrt{\sqrt{u} + 1} + 2, \tag{3.34}$$

$$x_4(u) = \sqrt{u} + 2\sqrt{\sqrt{u} + 1} + 2. \tag{3.35}$$

These are plotted as a function of the rotation parameter in figure (3.4). When behaviors of these roots are investigated, it can be observed that x_2 and x_4 are located outside of the event horizon. With the help of these solutions, the Lagrange-Bürmann method can be used to approximate solutions out of the equatorial plane for particles with unit energy.

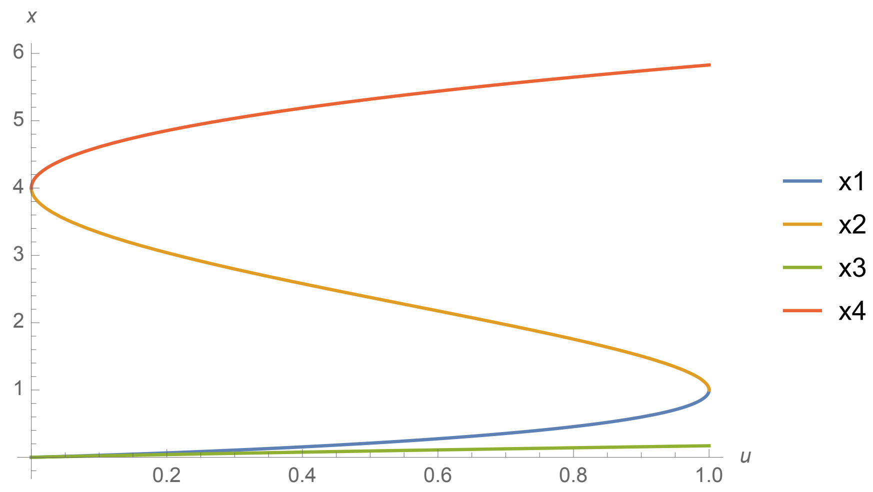

Figure 3.4: Roots of the polynomial on the equatorial plane for unit energy are plotted as a function of the rotation parameter.

3.5.2 Lagrange-Bürmann Method

The polynomial found in (3.27) is order of 2 with respect to ν. Hence, it has two solutions which are

$$\nu_1 = \frac{ux^2\left(u-x^2\right)\left(u+x(3x-4)\right) - 8\sqrt{u^2x^7(u+(x-2)x)^2}}{u^2\left(u^2+6ux^2+(9x-16)x^3\right)}, \tag{3.36}$$

and

$$\nu_2 = \frac{8\sqrt{u^2x^7(u+(x-2)x)^2} + ux^2\left(u-x^2\right)\left(u+x(3x-4)\right)}{u^2\left(u^2+6ux^2+(9x-16)x^3\right)}. \tag{3.37}$$

ν_2 is the root which approaches to 0 when $x = x_2$ or $x = x_4$. Therefore, it can be written as

$$\nu = \nu_2 = f(x) \tag{3.38}$$

and the Lagrange-Bürmann method allows us to estimate a funtion of the form

$$x = g(\nu), \tag{3.39}$$

where

$$\begin{aligned} g(\nu) &= x_2 + (\nu - f(x_2)) \lim_{x\to x_2}\left(\frac{x-x_2}{f(x)-f(x_2)}\right) \\ &\quad + \frac{(\nu - f(x_2))^2}{2} \lim_{x\to x_2}\left(\frac{d}{dx}\left(\frac{x-x_2}{f(x)-f(x_2)}\right)^2\right). \end{aligned} \tag{3.40}$$

Two conditions of the Lagrange-Bürmann inversion theorem, namely $f(x_2)$ should be analytic and $f'(x_2)$ should be nonzero, are satisfied. The error rate of the approximate solutions for different values of the rotation parameter at different inclination angles can be seen in the table (3.2). As can be observed, the approximation works quite well near the equatorial plane for the whole range of u. Nevertheless, near polar planes, a better approximation is needed.

Table 3.2: The error rates of the approximate solution obtained with the Lagrange-Bürmann method to the unit energy particle orbits.

ν	u	Error (%)
0.1	0.1	0.00128664
0.1	0.9	0.0298184
0.9	0.1	2.28609
0.9	0.9	20.3042

3.6 Other Energy Values

For energy values other than zero and unity, the polynomial (3.13) cannot be solved analytically in terms of a finite number of radicals even on the equatorial plane. Hence, in order to investigate the solutions with these energy values, a different approach should be devised.

3.6.1 Bound Orbits

At this point, a numerical analysis can be made to observe the behavior of bound orbits which have energy values between $k = 0$ and $k = 1$. Solutions on the equatorial plane are considered first.

As a first case, the rotation parameter is set equal to 0.1, $u = 0.1$, and the energy value is gradually decreased by starting with the unit energy, $k = 1$. With conditions $\nu = 0$ and $u = 0.1$, the polynomial equation (3.13) can be factored as

$$p(x) = x^4 \times p_1(x), \tag{3.41}$$

where

$$p_1(x) = x^6\left(k^2-2k+1\right)+x^5\left(-6k^2+14k-8\right) \quad (3.42)$$
$$+x^4\left(9k^2-32k+24\right)+x^3\left(-0.4k^2+24.6k-32.2\right)$$
$$+x^2\left(16.8-k\right)-0.8x+0.01.$$

The discriminant of $p_1(x)$ with respect to x has roots at $k = 0.864513$ and $k = 0.904746$. There are no real roots of the polynomial located outside of the event horizon for the interval where $0 < k < 0.864513$. There are two real roots in the interval $0.864512 < k < 0.904746$, and four real roots in the interval $0.904746 < k < 1$ of the polynomial which represent orbits located outside of the event horizon. The general behavior of the discriminant can be observed in the figure (3.5).

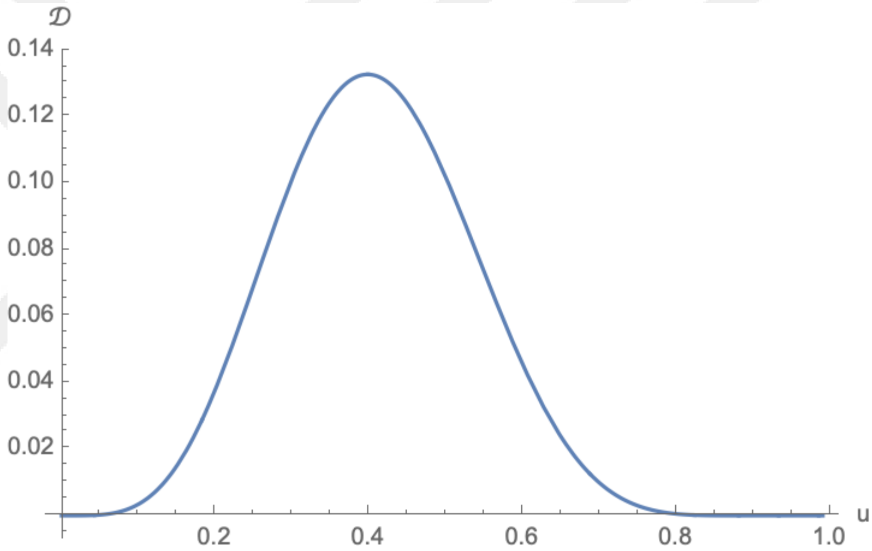

Figure 3.5: The graph of the discriminant of the polynomial with $\nu = 0$ and $u = 0.1$.

As a second case, the rotation parameter is set equal to 0.9, $u = 0.9$, and the energy value is gradually decreased by starting with the unit energy, $k = 1$. This time, the discriminant of the polynomial equation vanishes at $k = 0.657945$ and $k = 0.924715$. There are no real roots located outside of the event horizon for the interval $0 < k < 0.657945$. There are two real roots in the interval $0.657945 < k < 0.924715$, and there are four real roots in the interval $0.924715 < k < 1$ of the polynomial located outside of the event horizon. The behavior of the discriminant can be observed in figure (3.6) In figure (3.7), the distribution of the energy values, k, which makes the discriminant vanishes for all u values on the equatorial plane can be seen.

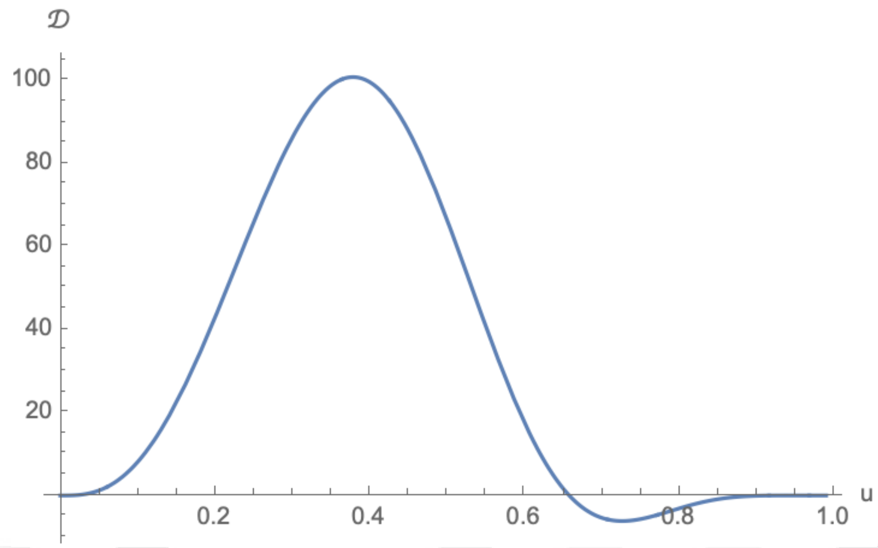

Figure 3.6: The graph of the discriminant of the polynomial with $\nu = 0$ and $u = 0.9$.

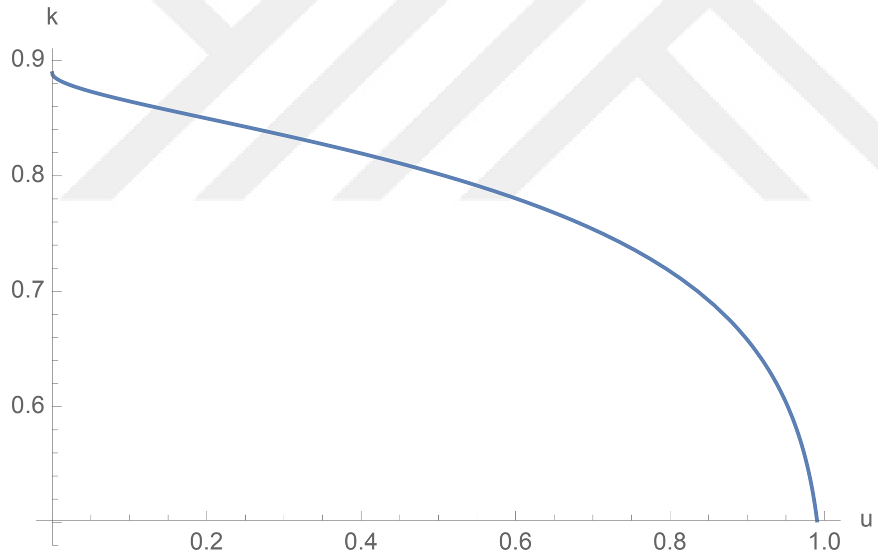

Figure 3.7: The graph of energy values, k, which make the discriminant vanish on the equatorial plane with respect to u.

As an another method to investigate the behavior of equatorial orbits with energy values between $k = 0$ and $k = 1$, the Lagrange-Bürmann method can be applied to the exact solution obtained for the unit energy at the equatorial plane in order to approximate the solution in the desired intervals where there is a real root outside the event horizon. The error rates for some specific cases are summarized in table (3.3).

Table 3.3: The error rates of the approximate solution obtained with the Lagrange-Bürmann method at the equatorial plane $\nu = 0$ for bound orbits.

u	k	Error (%)
0.1	0.9	3.03788
0.9	0.9	0.0726006
0.1	0.87	11.8191
0.9	0.87	0.173522

Now, the solutions on the polar plane can be investigated. With condition $\nu = 1$, the polynomial equation can be factored as

$$p(x) = p_1^2(x) \tag{3.43}$$

where

$$\begin{aligned} p_1(x) &= x^5(k-1) + x^4(4-3k) + x^3(2ku - 2u - 4) \\ &\quad + x^2(4u - 2ku) + x\left(ku^2 - u^2\right) + ku^2 \end{aligned} \tag{3.44}$$

As a first case, the rotation parameter is set equal to 0.1, $u = 0.1$, and the energy value is gradually decreased by starting with the unit energy, $k = 1$. The discriminant of $p_1(x)$ with respect to x has a root at $k = 0.888049$. There are real roots of the polynomial located outside of the event horizon for the interval where $0.888049 < k \leq 1$ and for the special case $k = 0$. This time, there are other real roots of the discriminant in the interval $0 \leq k < 0.888049$, but they only affect the number of real orbits located inside the event horizon. The behavior of the discriminant can be seen in figure (3.8).

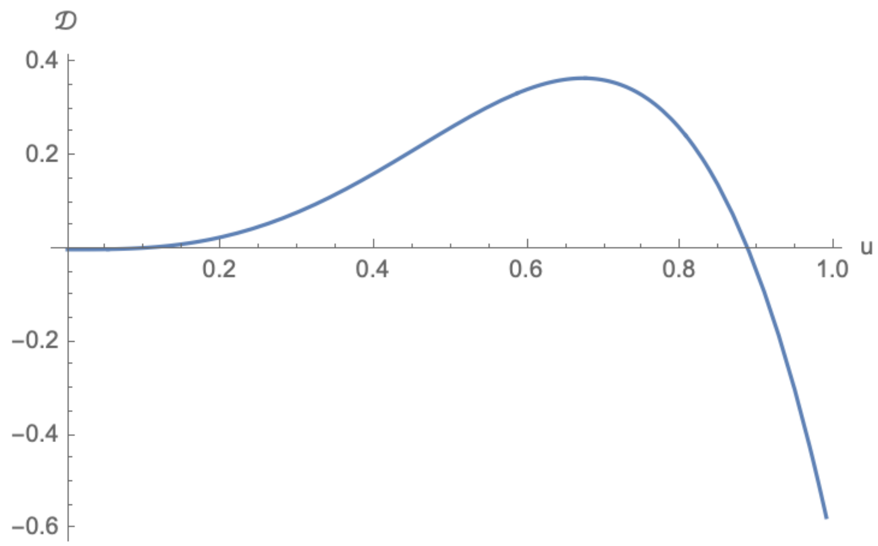

Figure 3.8: The graph of the discriminant of the polynomial with $\nu = 1$ and $u = 0.1$.

As a second case, the rotation parameter is set equal to 0.9, $u = 0.9$ and the energy value is gradually decreased by starting with the unit energy, $k = 1$. The discriminant of the polynomial equation vanishes at the point where $k = 0.879759$. There are real roots located outside of the event horizon for the interval $0.879759 < k \leq 1$ and for the special case $k = 0$. The general behavior of the discriminant can be observed in figure (3.9). In figure (3.10), the distribution of the energy values, k, which make the discriminant vanish for all u values on the polar plane can be seen.

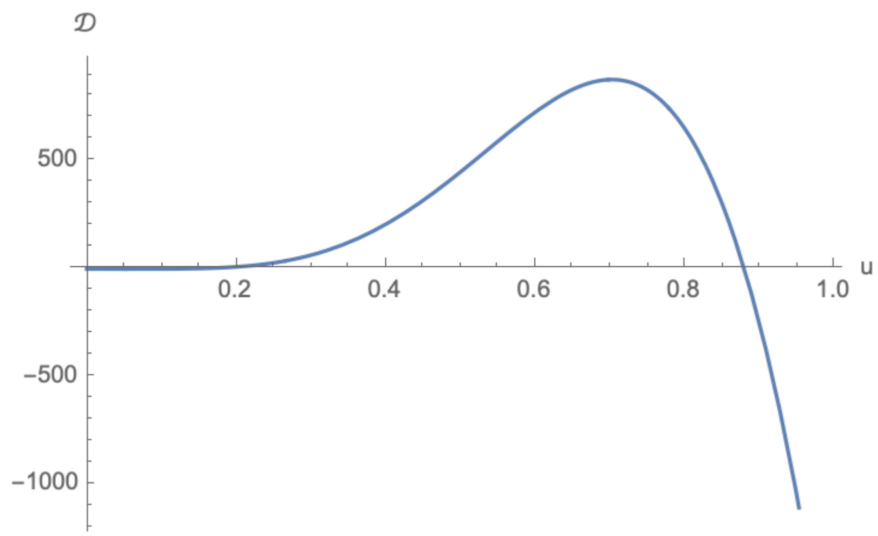

Figure 3.9: The graph of the discriminant of the polynomial with $\nu = 1$ and $u = 0.9$.

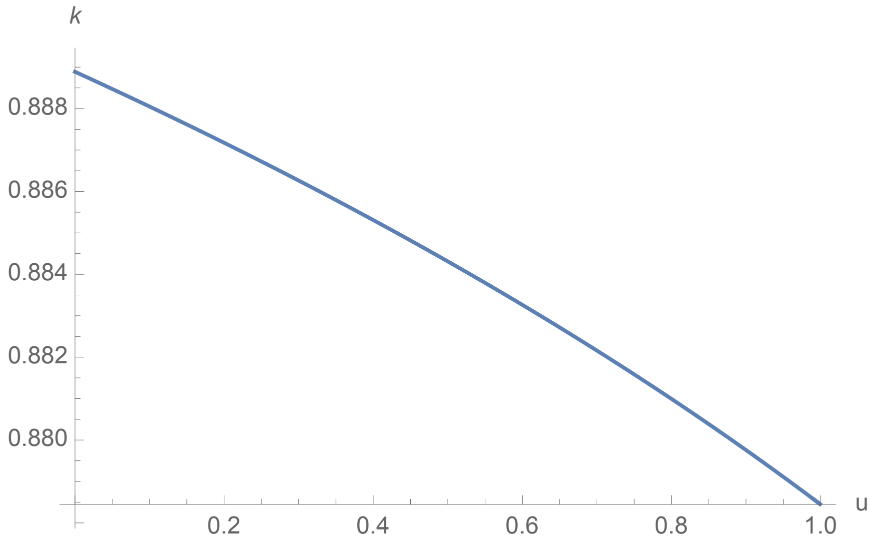

Figure 3.10: The graph of energy values, k, which makes the discriminant vanish on the polar plane with respect to u.

Approximate solutions to investigate the behavior of polar orbits with energy values which are in the interval where there is a real root outside of the event horizon, can be obtained with the help of the Lagrange-Bürmann method. The error rates for some specific cases are shown in table (3.4).

Table 3.4: The error rates of the approximate solution obtained with the Lagrange-Bürmann method at the polar plane $\nu = 1$ for bound orbits.

u	k	Error (%)
0.1	0.9	2.9904
0.9	0.9	1.70533
0.1	0.89	9.12136
0.9	0.89	4.01093

3.6.2 Unbound Orbits

The approach used for bound orbits with energy values $k < 1$ can be used for unbound orbits with energy values $k > 1$. As a first case, equatorial plane solutions are investigated. This time there is no limit observed on the energy levels. In other words, there always exist real orbits outside the event horizon for energy values $k > 1$. The exact solutions obtained on the equatorial plane can be used to approximate solutions on planes with the critical inclination angle greater than zero, $\nu > 0$ with the help of the Lagrange-Bürmann method. The error rates of some specific cases are summarized in table (3.5).

Table 3.5: The error rates of the approximate solution obtained with the Lagrange-Bürmann method at the equatorial plane, $\nu = 0$ for unbound orbits.

u	k	Error (%)
0.1	1.1	1.04468
0.9	1.1	0.0477497
0.1	1.5	24.1319
0.9	2	19.2937

As a second case polar plane solutions are investigated. Again, there is no limit on k. The exact solutions of the polar plane for $k = 1$ can be used to approximate solutions on planes with critical inclination angle $\nu < 1$ with the help of the Lagrange-Bürmann method. The error rates for some specific cases are shown in table (3.6).

Table 3.6: The error rates of the approximate solution obtained with the Lagrange-Bürmann method at the polar plane, $\nu = 1$ for unbound orbits.

u	k	Error (%)
0.1	1.1	0.536127
0.9	1.1	0.392406
0.1	1.2	25.2596
0.9	1.2	18.784

CHAPTER 4

EVENT HORIZON DETECTING INVARIANTS

4.1 Curvature invariants of the hypersurface

The method developed here, which works for the BTZ black hole and other black holes in three, four, and five dimensions, is a variant of the method of Page and Shoom [26], but only uses one curvature invariant. Beyond five dimensions, the method will still be valid, but one needs more than one curvature invariant as such, it is not more advantageous than the method of [26], which also generically requires more than one curvature invariant.

The main idea of the proposal is as follows: as was realized in [26] in a spacetime with a stationary black hole, there is always a symmetry that can be used to split the tangent space of the spacetime into two parts. Let G be the local symmetry group with m dimensional maximal orbits. Hence the local cohomogeneity has $n = D - m$ dimensions. Considering a set of gradients $\{dS^i\}$ built from n functionally independent nonconstant curvature scalars, their wedge product, say W, (which is proportional to the volume form on the cohomogeneity space) will vanish on the event horizon since the Hodge dual of W vanishes there. This can be used to detect the event horizon. However, clearly, for the case of the BTZ black hole, there is no such non-constant curvature scalar. One possible way out of this problem is to reduce the local cohomogeneity. Especially, if the local cohomogeneity can be reduced to one, just one curvature invariant, which vanishes on the horizon, can be used. In order to reduce the local cohomogeneity, the $D - 1$ dimensional surface Σ is embedded to the D-dimensional spacetime. It is essential to understand that this Σ is not the event horizon $\mathcal{H}$. Let us carry out this procedure for the BTZ black hole first and then to other black holes.

4.2 BTZ Black Hole

In (t, r, ϕ) coordinates, the BTZ metric is given as

$$g_{\mu\nu} = \begin{pmatrix} m - \frac{r^2}{\ell^2} & 0 & -\frac{j}{2} \\ 0 & \frac{1}{\frac{j^2}{4r^2}+\frac{r^2}{\ell^2}-m} & 0 \\ -\frac{j}{2} & 0 & r^2 \end{pmatrix}, \tag{4.1}$$

where m and j are mass and angular momentum, respectively; and ℓ is the AdS_3 radius. In this coordinate system, the coordinates t, and ϕ have associated Killing symmetries, ∂_t and ∂_ϕ respectively. The event horizon can be easily found as the largest root of $g^{rr} = 0$ or equivalently as the location at which the time-like Killing vector $\xi = \partial_t + \Omega\partial_\phi$ becomes null where $\Omega = -g_{t\phi}/g_{\phi\phi}$ which becomes $\Omega = j/(2r_+^2)$ at the event horizon. Both results yield

$$r_\pm^2 = \frac{m\ell^2}{2}\left(1 \pm \sqrt{1 - \frac{j^2}{\ell^2 m^2}}\right), \tag{4.2}$$

with the positive root giving the event horizon.

Let us now find this in a coordinate independent way. The cohomogeneity of this spacetime is one. Keeping this intact, a hypersurface which has at least one non-constant curvature invariant is needed to be chosen. For this purpose, the $t = t_0$ or the $\phi = \phi_0$ can be chosen to define the hypersurface (note again that it is not the event horizon itself). Both options are valid and yield the same result, let us choose the latter, then the induced metric becomes

$$\gamma_{ij} = \begin{pmatrix} m - \frac{r^2}{\ell^2} & 0 \\ 0 & \frac{1}{\frac{j^2}{4r^2}+\frac{r^2}{\ell^2}-m} \end{pmatrix} \tag{4.3}$$

in the induced coordinates (t, r). This metric has a symmetry only in the t coordinate. So, the cohomogeneity is still one, as expected. The Kretschmann invariant computed for the induced metric (4.3) becomes,

$$^{\Sigma}I_1 = {}^{\Sigma}R_{ijkl}{}^{\Sigma}R^{ijkl} = \frac{\left(j^2\ell^2 - 4\left(r^2 - \ell^2 m\right)^2\right)^2}{4\left(\ell^3 m - \ell r^2\right)^4}, \tag{4.4}$$

from which one can calculate the horizon detecting invariant

$$ {}^{\Sigma}I_5 = \nabla_m {}^{\Sigma}I_1 \nabla^{m\Sigma} I_1, \tag{4.5} $$

which reads explicitly as

$$ {}^{\Sigma}I_5 = \frac{j^4\left(j^2\ell^2 - 4\ell^2 m r^2 + 4r^4\right)\left(j^2\ell^2 - 4\left(r^2-\ell^2 m\right)^2\right)^2}{\ell^6\left(r^2-\ell^2 m\right)^{10}}, \tag{4.6} $$

whose largest real root, $I_5(r=r_+)=0$, is exactly the event horizon given as 4.2.

In fact for the BTZ black hole, the hypersurface version of the curvature invariant given in [25] can also be used to detect the event horizon as a somewhat simpler way. One can show that for the hypersurface metric (4.3), one has

$$ \begin{aligned} {}^{\Sigma}I_3 &= \nabla_m {}^{\Sigma}R_{ijkl} \nabla^{m\Sigma} R^{ijkl} \\ &= \frac{j^4\left(j^2\ell^2 - 4\ell^2 m r^2 + 4r^4\right)}{\ell^2\left(r^2-\ell^2 m\right)^6}, \end{aligned} \tag{4.7} $$

which vanishes only on the event horizon and on the inner horizon. Therefore, it is a very useful tool for event horizon detection.

4.3 Warped AdS_3 black hole

The method described above is geometric, in the sense that it relies on the metric and not on the underlying field equations. Therefore, it can be applied to other metrics that solve field equations that are different from general relativity. Let us consider the case of the warped AdS_3 black hole in the (t, r, ϕ) coordinates [38, 39, 40].

$$ \begin{aligned} ds^2 = \quad & -\ell^2 dt^2 + \frac{\ell^2}{\left(\nu^2+3\right)(r-p)(r-q)} dr^2 + \\ & + \frac{1}{4}\ell^2 r f d\phi^2 - \ell^2\left(\sqrt{pq\left(\nu^2+3\right)} - 2r\nu\right) dt d\phi, \end{aligned} \tag{4.8} $$

where the function f is given as

$$ f := \left(\nu^2+3\right)(p+q) - 4\nu\sqrt{pq\left(\nu^2+3\right)} + 3r\left(\nu^2-1\right). $$

The event horizon is at $r_+ = p$, and the inner horizon is at $r_- = q$. This metric solves the topologically massive gravity [41] for $\nu = \mu\frac{\ell}{3}$

$$ R_{\mu\nu} - \frac{1}{2}R g_{\mu\nu} - \frac{1}{\ell^2} + \frac{1}{\mu}C_{\mu\nu} = 0, \tag{4.9} $$

where $C_{\mu\nu}$ is the Cotton tensor and μ is the topological mass. Even though the Ricci tensor and the Riemann tensor of this spacetime are different forms of the maximally symmetric AdS_3, the curvature invariants of the full spacetime cannot detect the event horizon because all the curvature scalars are constant. In fact, explicit forms of some of the curvature invariants are given as

$$\begin{aligned} R_{\mu\nu\rho\sigma}R^{\mu\nu\rho\sigma} &= \frac{12\left(2\nu^4-4\nu^2+3\right)}{\ell^4}, \\ R_{\mu\nu}R^{\mu\nu} &= \frac{6\left(\nu^4-2\nu^2+3\right)}{\ell^4}, \\ \nabla_\sigma R_{\mu\nu}\nabla^\sigma R^{\mu\nu} &= -\frac{36\nu^2\left(\nu^2-1\right)^2}{\ell^6}, \\ \nabla_\sigma R_{\mu\nu\rho\gamma}\nabla^\sigma R^{\mu\nu\rho\gamma} &= -\frac{144\nu^2\left(\nu^2-1\right)^2}{\ell^6}, \end{aligned} \tag{4.10}$$

which are not useful to detect the event horizon. Therefore our method can be resorted, but there is a subtle issue here. As in the case of the BTZ black hole, there are two Killing symmetries for the warped AdS_3 black hole and two possible ways of choosing the hypersurface by keeping the cohomogeneity constant. However, only one of these two ways yields a hypersurface with non-constant curvature invariants. In fact, if the hypersurface is defined as $\phi = \phi_0$, a flat metric will be obtained, that is not useful at all. The other option, that is choosing the hypersurface defined by $t = t_0$, yields a nontrivial result. The induced metric is

$$ds_\Sigma^2 = \frac{\ell^2}{\left(\nu^2+3\right)(r-p)(r-q)}dr^2 + \frac{1}{4}\ell^2 r f d\phi^2 \tag{4.11}$$

in the induced coordinates (r, ϕ).

Now, the relevant invariants can be calculated as given by (4.5) and/or (4.7) as both invariants work as in the case of the BTZ metric. The explicit expressions are cumbersome, hence they are depicted in Appendix G; but note that, they both vanish on the event horizon, i.e.

$${}^\Sigma I_5(r = r_+) = 0, \tag{4.12}$$

$${}^\Sigma I_3(r = r_+) = 0. \tag{4.13}$$

4.4 Two examples in 2+1 dimensions

In 2+1 dimensions, there is a purely quadratic gravity theory (the so called K-gravity) defined by the action [42]

$$S=\int d^3x\sqrt{-g}\left(R_{\mu\nu}R^{\mu\nu}-\frac{3}{8}R^2\right), \tag{4.14}$$

that admits asymptotically flat and rotating black holes [43, 44]. Let us apply the above procedure to detect the event horizons of these black holes.

4.4.1 Asymptotically flat solution of K-gravity

The metric is given as

$$ds^2=-\left(br-\mu\right)dt^2+\frac{1}{br-\mu}dr^2+r^2d\phi^2. \tag{4.15}$$

The usual method shows that there is an event horizon at $r=\mu/b$, as is clear from the metric. This spacetime has two symmetries and has cohomogeneity one which admits two possible hypersurfaces. But one of these, that is reducing along the ϕ coordinate, yields a flat space and hence, it is not a viable option. So, the hypersurface defined by $t=t_0$ is chosen. Then the relevant invariants (4.5) and (4.7) read as

$${}^{\Sigma}I_5=\frac{4b^4(br-\mu)}{r^6}, \tag{4.16}$$

and

$${}^{\Sigma}I_3=\frac{b^2(br-\mu)}{r^4}, \tag{4.17}$$

which vanish on the horizon.

4.4.2 Rotating solution of K-gravity

The following metric which describes a rotating black hole also solves the K-gravity [43]

$$\begin{aligned} ds^2 &= (\mu-br)du^2-2\sqrt{\frac{\left(a^2b+8r\right)^2}{a^4b^2+16a^2\mu+64r^2}}dudr \\ &\quad +a(\mu-br)dud\phi+\left(\frac{a^4b^2}{64}+\frac{a^2\mu}{4}+r^2\right)d\phi^2. \end{aligned} \tag{4.18}$$

The cohomogeneity of this spacetime is one. Therefore, the event horizon can be detected by using the curvature invariants ${}^{\Sigma}I_5$ (4.5) and/or, ${}^{\Sigma}I_3$ (4.7). The spacetime can be induced on the constant ϕ_0 hypersurface which has

$$\begin{aligned} {}^{\Sigma}I_5 &= \frac{16777216a^8b^4(br-\mu)\left(a^2b^2-8br+16\mu\right)^2}{\left(a^2b+8r\right)^{16}} \\ &\quad\times\left(a^2b^2-4br+12\mu\right)^2\left(a^4b^2+16a^2\mu+64r^2\right), \end{aligned} \tag{4.19}$$

and

$$\begin{aligned} {}^{\Sigma}I_3 &= \frac{65536a^4b^2(br-\mu)\left(a^2b^2-4br+12\mu\right)^2}{\left(a^2b+8r\right)^{10}} \\ &\quad\times\left(a^4b^2+16a^2\mu+64r^2\right). \end{aligned} \tag{4.20}$$

Both invariants vanish, for real values of r, on the event horizon $r = \mu/b$ and change sign there. They also vanish for some other values of r but at these points there is no change of sign.

4.5 Kerr Black Hole

Let us apply the above reasoning to the four dimensional Kerr black hole [10], which has two Killing symmetries. Therefore, the cohomogeneity of this spacetime is two. By choosing some special hypersurfaces, the cohomogeneity can be reduced to one.

The components of the Kerr metric in the Boyer-Lindquist coordinates (t, r, X, ϕ) is

$$\begin{aligned} ds^2 &= -(1-\frac{2mr}{\rho^2})dt^2 - \frac{4amr(1-X^2)}{\rho^2}dtd\phi \\ &\quad+(r^2+a^2+\frac{2a^2mr(1-X^2)}{\rho^2})(1-X^2)d\phi^2 \\ &\quad+\frac{\rho^2}{\Sigma}dr^2+\frac{\rho^2}{1-X^2}dX^2, \end{aligned} \tag{4.21}$$

where $\rho^2 = r^2 + a^2X^2$, $\Sigma = r^2 - 2mr + a^2$, $X = \cos\theta$, and m and a correspond to mass and the rotation parameter, respectively. The hypersurface that will be embedded into the spacetime is defined by,

$$p \in M, \qquad p \in \Sigma \iff X(p) = X_0 = \text{constant}. \tag{4.22}$$

The induced metric on the hypersurface can be found by pulling it back from the spacetime metric. The components of it can be written with respect to the induced coordinates (t, r, ϕ) as

$$
\begin{aligned}
ds^2_\Sigma &= -(1-\frac{2mr}{\rho^2})dt^2 - \frac{4amr(1-X_0^2)}{\rho^2}dtd\phi \\
&\quad +(r^2+a^2+\frac{2a^2mr(1-X_0^2)}{\rho^2})(1-X_0^2)d\phi^2 + \frac{\rho^2}{\Sigma}dr^2.
\end{aligned} \tag{4.23}
$$

The Kretschmann scalar

$$
{}^\Sigma I_1 = {}^\Sigma R_{ijkl}{}^\Sigma R^{ijkl} \tag{4.24}
$$

of the hypersurface can be found, from which one can compute

$$
{}^\Sigma I_5 = \quad \nabla_\mu{}^\Sigma I_1 \nabla^{\mu\Sigma} I_1, \tag{4.25}
$$

which for $X_0 = 0$ yields

$$
{}^\Sigma I_5 = \frac{20736M^4\left(a^2+r(r-2M)\right)}{r^{16}}, \tag{4.26}
$$

that vanishes on the event horizon given as $r_+ = m + \sqrt{m^2-a^2}$, which matches the result of the coordinate dependent method. The explicit forms of these curvature invariants provided in Appendix H.

Let us stress that instead of the hypersurface construction given above, if the full spacetime invariant given as

$$
I_5 = \nabla_\mu I_1 \nabla^\mu I_1 \tag{4.27}
$$

had been used, the event horizon could not have been detected with this invariant alone. Therefore, in this approach, a simplified way to detect the horizon is obtained. Another advantage of this approach is that, when it is calculated in the $X(p) = X_0 = 0$ hypersurface, the invariant vanishes *only* on the event horizon of the black hole and there are no other roots at finite r. In the method of [26], the norm of the wedge square have other roots in addition to the root indicating the horizon.

4.6 4+1 Myers-Perry Black Hole

Myers and Perry [45] found the rotating, massive, Ricci flat black holes in generic $D \geq 5$ dimensions. Here, as an example, the five dimensional solution that can be studied with the method developed above with the help of a single curvature invariant is considered. In this spacetime, the coordinates are chosen as $(t, r, X, \phi_1, \phi_2)$ where $X = \cos\theta$. The metric is then,

$$\begin{aligned} ds^2 &= -dt^2 + \frac{m}{\Sigma}\left(dt + k(1-X^2)d\phi_1 + lX^2 d\phi_2\right)^2 + \frac{r^2\Sigma}{\Pi - mr^2}dr^2 \\ &\quad + \frac{\Sigma}{1-X^2}dX^2 + (r^2+k^2)(1-X^2)d\phi_1^2 + (r^2+l^2)X^2 d\phi_2^2, \end{aligned} \tag{4.28}$$

where

$$\begin{aligned} \Sigma &= r^2 + k^2X^2 + l^2(1-X^2), \\ \Pi &= (r^2+k^2)(r^2+l^2). \end{aligned} \tag{4.29}$$

Here k and l are angular momentum parameters as there are two possible independent angular momenta in five dimensions. In this coordinate system, the coordinates t, ϕ_1, ϕ_2 have associated symmetries. Hence, the cohomogeneity of this spacetime is two. The spacetime can be induced onto the hypersurface of constant X, let say X_0. Then, the induced metric is

$$\begin{aligned} ds_\Sigma^2 &= -dt^2 + \frac{m}{\Sigma}(dt + k(1-X_0^2)d\phi_1 + lX_0^2 d\phi_2)^2 \\ &\quad + \frac{r^2\Sigma}{\Pi - mr^2}dr^2 + (r^2+k^2)(1-X_0^2)d\phi_1^2 + (r^2+l^2)X_0^2 d\phi_2^2 \end{aligned} \tag{4.30}$$

in the induced coordinates (t, r, ϕ_1, ϕ_2). Again, one computes the Kretschmann invariant of this hypersurface from which one computes (4.5). The explicit forms of the expressions are complicated, therefore they are provided in Appendix I, but one can show that ${}^\Sigma I_5 = 0$ at

$$r_+ = \frac{\sqrt{\sqrt{(k^2+l^2-m)^2 - 4k^2l^2} - k^2 - l^2 + m}}{\sqrt{2}} \tag{4.31}$$

which is the location of the event horizon.

CHAPTER 5

CONCLUSIONS

In this thesis, some of the crucial aspects of black holes have been investigated. In the second chapter, the motion of light in the vicinity of a Kerr black hole is analyzed. Up to now, the radii of the polar and the equatorial plane light orbits have been known explicitly in terms of the rotation parameter of the black hole. Here, the known analytical solutions have been extended by showing that there are two exterior nonequatorial light orbits whose radii can be found analytically for a given black hole with a rotation parameter a. One of these orbits is a prograde orbit, which monotonically decreases in the rotation parameter and the other one is a retrograde orbit, which is nonmonotonic, in contrast to the equatorial retrograde orbit that is monotonic. This feature was observed in [35] for the extremal black hole case. The effective inclination angle of these two orbits is critical in the sense that exactly at and below that angle, there are always four spherical null orbits. Two of these are inside the event horizon, and at the critical angle, these two orbits merge into a single orbit with a radius, which can be analytically expressed in terms of the rotation parameter. These two interior exact solutions, which are presumably not significant for astrophysics, may nevertheless be important to better explore the geometry of the black hole region. The novel solutions presented here are all unstable in the radial direction, as all the spherical geodesics are unstable; this fact is closely related to the stability and the shadow of the Kerr black hole [46].

In the third chapter, the method developed for spherical photon orbits has been extended to cover timelike orbits of massive particles around Kerr black hole. For zero energy particles, a non-monotonicity has been observed in the retrograde orbits. The farthest point to which a retrograde orbit can reach has been calculated with the help of the discriminant of the sextic polynomial equation. A numerical analysis has been applied to find out whether this non-monotonic behaviour occurs for retrograde orbits of particles with nonzero energy. It has been observed that the non-monotonicity in retrograde orbit is a common property of particles with both zero and nonzero energies only at high inclination angle values. A formula has been derived to detect the critical inclination angle above which non-monotonicity starts. The equatorial plane and the polar plane orbits of unit energy particles are explicitly investigated. Two approximate solutions have been developed. One of them helps to investigate the non-equatorial and non-polar orbits of unit energy particles. The other approximate solution helps to investigate the equatorial and polar orbits of particles with energy values $0 < E < 1$ and $1 < E$.

In the fourth chapter, inspired by the recent progress [24] in defining the event horizon of black holes with curvature invariants in $D = 4$ dimensions and $D \geq 4$ dimensions [26], a method which also works for $D = 3$ spacetime dimensions has been presented. The method of Page and Shoom makes use of the invariants of full spacetime that works well unless the invariants are all constant as in the case of three-dimensional BTZ black hole. The method developed here adapts their idea, but instead of using the invariants of the full spacetime, the invariants of well-chosen hypersurfaces have been used. Several examples in three, four and five dimensions have been given where only one invariant to detect the black hole horizon is needed. Beyond five dimensions, just like the method of [26], generically with our method, more than one horizon detecting invariant has been needed because usually the cohomogeneity is more than two. For more on the construction of horizon detecting invariants see [47] where Cartan invariants are suggested.

REFERENCES

[1] C. Montgomery, W. Orchiston, and I. Whittingham, “Michell, Laplace and the origin of the black hole concept,” *Journal of Astronomical History and Heritage*, vol. 12, pp. 90–96, July 2009.

[2] J. Michell, “On the means of discovering the distance, magnitude, &c. of the fixed stars, in consequence of the diminution of the velocity of their light, in case such a diminution should be found to take place in any of them, and such other data should be procured from observations, as would be farther necessary for that purpose. by the rev. john michell, b. d. f. r. s. in a letter to henry cavendish, esq. f. r. s. and a. s.,” *Philosophical Transactions of the Royal Society of London*, vol. 74, pp. 35–57, 1784.

[3] S. W. Hawking and G. F. R. Ellis, *Translation of an essay by P. S. Laplace*, p. 365–368. Cambridge Monographs on Mathematical Physics, Cambridge University Press, 1973.

[4] R. W. Smith, “The cambridge network in action: The discovery of neptune,” *Isis*, vol. 80, no. 3, pp. 395–422, 1989.

[5] M. Grosser, *The Discovery of Neptune*. Dover Books Explaining Science, Harvard University Press, 1962.

[6] S. Weinberg, *Gravitation and Cosmology: Principles and Applications of the General Theory of Relativity*. New York: John Wiley and Sons, 1972.

[7] A. Einstein, “Explanation of the Perihelion Motion of Mercury from the General Theory of Relativity,” *Sitzungsberichte der Preussischen Akademie der Wissenschaften. Physikalisch-Mathematische Klasse.*, vol. 1915, pp. 831–839, 1915.

[8] G. A. Lemaître and M. A. H. MacCallum, “The Expanding Universe,” *General Relativity and Gravitation*, vol. 29, pp. 641–680, May 1997.

[9] D. Finkelstein, "Past-future asymmetry of the gravitational field of a point particle," *Physical Review*, vol. 110, pp. 965–967, May 1958.

[10] R. P. Kerr, "Gravitational field of a spinning mass as an example of algebraically special metrics," *Physical Review Letters*, vol. 11, pp. 237–238, Sep 1963.

[11] E. L. Schucking, "The first Texas symposium on relativistic astrophysics," *Physics Today*, vol. 42, pp. 46–52, Aug. 1989.

[12] E. T. Newman, E. Couch, K. Chinnapared, A. Exton, A. Prakash, and R. Torrence, "Metric of a Rotating, Charged Mass," *Journal of Mathematical Physics*, vol. 6, pp. 918–919, June 1965.

[13] R. Kerr, "Discovering the kerr and kerr-schild metrics," *arXiv: General Relativity and Quantum Cosmology*, 2007.

[14] R. Penrose, "Gravitational collapse and space-time singularities," *Physical Review Letters*, vol. 14, pp. 57–59, Jan 1965.

[15] H. M. Hill, "The theory of black hole formation shares the nobel prize in physics," *Physics Today*, vol. 73, pp. 14–17, 2020.

[16] E. Gourgoulhon and J. L. Jaramillo, "A 3+1 perspective on null hypersurfaces and isolated horizons," *Physics Reports*, vol. 423, no. 4, pp. 159–294, 2006.

[17] A. Tavlayan and B. Tekin, "Exact formulas for spherical photon orbits around kerr black holes," *Physical Review D*, vol. 102, p. 104036, Nov 2020.

[18] B. P. Abbott *et al.*, "Observation of gravitational waves from a binary black hole merger," *Physical Review Letters*, vol. 116, p. 061102, Feb 2016.

[19] R. Abbott *et al.*, "GW190521: A Binary Black Hole Merger with a Total Mass of $150M_\odot$," *Physical Review Letters*, vol. 125, no. 10, p. 101102, 2020.

[20] K. Akiyama *et al.*, "First M87 Event Horizon Telescope Results. I. The Shadow of the Supermassive Black Hole," *Astrophysical Journal Letters*, vol. 875, p. L1, 2019.

[21] P. V. P. Cunha and C. A. R. Herdeiro, "Stationary black holes and light rings," *Physical Review Letters*, vol. 124, no. 18, p. 181101, 2020.

[22] E. Teo, "Spherical photon orbits around a kerr black hole," *General Relativity and Gravitation*, vol. 35, pp. 1909–1926, 11 2003.

[23] A. Tavlayan and B. Tekin, "Event horizon detecting invariants," *Physical Review D*, vol. 101, p. 084034, Apr 2020.

[24] M. Abdelqader and K. Lake, "Invariant characterization of the kerr spacetime: Locating the horizon and measuring the mass and spin of rotating black holes using curvature invariants," *Physical Review D*, vol. 91, p. 084017, Apr 2015.

[25] A. Karlhede, U. Lindstrom, and J. E. Aman, "A note on a local effect at the Schwarzschild sphere," *General Relativity and Gravitation*, vol. 14, pp. 569–571, June 1982.

[26] D. N. Page and A. A. Shoom, "Local invariants vanishing on stationary horizons: A diagnostic for locating black holes," *Physical Review Letters*, vol. 114, p. 141102, Apr 2015.

[27] M. Bañados, C. Teitelboim, and J. Zanelli, "Black hole in three-dimensional spacetime," *Physical Review Letters*, vol. 69, pp. 1849–1851, Sep 1992.

[28] B. Carter, "Global structure of the kerr family of gravitational fields," *Physical Review*, vol. 174, pp. 1559–1571, Oct 1968.

[29] C. W. Misner, K. S. Thorne, and J. A. Wheeler, *Gravitation*. San Francisco: W. H. Freeman, 1973.

[30] F. D. Ryan, "Effect of gravitational radiation reaction on circular orbits around a spinning black hole," *Physical Review D*, vol. 52, pp. R3159–R3162, Sep 1995.

[31] J. M. Bardeen, W. H. Press, and S. A. Teukolsky, "Rotating black holes: Locally nonrotating frames, energy extraction, and scalar synchrotron radiation," *Astrophysical Journal*, vol. 178, p. 347, 1972.

[32] T. Jacobson, "Where is the extremal Kerr ISCO?," *Classical and Quantum Gravity*, vol. 28, p. 187001, 2011.

[33] H. Mellin, "Résolution de l'équation algébrique généralea l'aide de la fonction gamma," *Comptes Rendus de l'Académie des Sciences - Series I - Mathematics*, vol. 172, pp. 658–661, 1921.

[34] H. Umemura and D. Mumford, *Resolution of algebraic equations by theta constants*, pp. 3261–3272. Birkhäuser, 1984.

[35] S. Hod, “Spherical null geodesics of rotating kerr black holes,” *Physics Letters B*, vol. 718, no. 4, pp. 1552–1556, 2013.

[36] P. Henrici, *Applied and Computational Complex Analysis, Volume 1: Power Series Integration Conformal Mapping Location of Zero*. Wiley Classics Library, Wiley, 1988.

[37] A. Grib and Y. Pavlov, “Black holes and particles with zero or negative energy,” *Theoretical and Mathematical Physics*, vol. 190, pp. 268–278, 2016.

[38] Y. Nutku, “Exact solutions of topologically massive gravity with a cosmological constant,” *Classical and Quantum Gravity*, vol. 10, pp. 2657–2661, dec 1993.

[39] M. Gürses, “Perfect Fluid Sources in 2+1 Dimensions,” *Classical and Quantum Gravity*, vol. 11, no. 10, p. 2585, 1994.

[40] D. Anninos, W. Li, M. Padi, W. Song, and A. Strominger, “Warped AdS3black holes,” *Journal of High Energy Physics*, vol. 2009, pp. 130–130, mar 2009.

[41] S. Deser, R. Jackiw, and S. Templeton, “Topologically Massive Gauge Theories,” *Annals of Physics*, vol. 140, pp. 372–411, 1982. [Erratum: Annals Phys. 185, 406 (1988)].

[42] S. Deser, “Ghost-free, finite, fourth-order $d = 3$ gravity,” *Physical Review Letters*, vol. 103, p. 101302, Sep 2009.

[43] G. Barnich, C. Troessaert, D. Tempo, and R. Troncoso, “Asymptotically locally flat spacetimes and dynamical nonspherically-symmetric black holes in three dimensions,” *Physical Review D*, vol. 93, p. 084001, Apr 2016.

[44] G. Alkaç, E. Kilicarslan, and B. Tekin, “Asymptotically flat black holes in 2+1 dimensions,” *Physical Review D*, vol. 93, no. 8, p. 084003, 2016.

[45] R. C. Myers and M. J. Perry, “Black Holes in Higher Dimensional Space-Times,” *Annals of Physics*, vol. 172, p. 304, 1986.

[46] P. V. P. Cunha, C. A. R. Herdeiro, and E. Radu, "Fundamental photon orbits: Black hole shadows and spacetime instabilities," *Physical Review D*, vol. 96, p. 024039, Jul 2017.

[47] D. D. McNutt, M. A. H. MacCallum, D. Gregoris, A. Forget, A. A. Coley, P. C. Chavy-Waddy, and D. Brooks, "Cartan Invariants and Event Horizon Detection, Extended Version," *General Relativity and Gravitation*, vol. 50, no. 4, p. 37, 2018. [Erratum: Gen.Rel.Grav. 52, 6 (2020)].

[48] I. Herstein, *Topics in Algebra*. Xerox College Pub., 1975.

[49] P. Ramond, "Abel-ruffini's theorem: Complex but not complicated!," *arXiv: History and Overview*, 2020.

[50] R. Garver, "The Tschirnhaus transformation," *Annals of Mathematics*, vol. 29, no. 1/4, pp. 319–333, 1927.

[51] J. V. Armitage and W. F. Eberlein, *Elliptic Functions*. London Mathematical Society Student Texts, Cambridge University Press, 2006.

[52] N. Bagis, "Solution of polynomial equations with nested radicals," *arXiv: General Mathematics*, 2014.

[53] A. Akritas and A. Akritas, *Elements of Computer Algebra With Applications*. A Wiley-Interscience publication, Wiley, 1989.

[54] N. Grossman, "A c^{∞} lagrange inversion theorem," *The American Mathematical Monthly*, vol. 112, no. 6, pp. 512–514, 2005.

[55] E. Whittaker and G. Watson, *A Course of Modern Analysis*. A Course of Modern Analysis: An Introduction to the General Theory of Infinite Processes and of Analytic Functions, with an Account of the Principal Transcendental Functions, Cambridge University Press, 1996.

[56] M. Abramowitz and I. Stegun, *Handbook of Mathematical Functions: With Formulas, Graphs, and Mathematical Tables*. Applied mathematics series, Dover Publications, 1965.

APPENDIX A

DERIVATION OF SEXTIC POLYNOMIAL

Recall that with the help of two conditions, $R(r) = 0$ and $\frac{dR(r)}{dr} = 0$, on the radial part of the geodesic equation, two physically viable equations were obtained, (2.11) and (2.12). These equations can be combined into a single equation by using *effective inclination angle*, (3.8),

$$\nu \equiv \sin^2 i = \frac{\mathcal{Q}}{L_z^2 + \mathcal{Q}} = -\frac{r^3 \left(r^3 - 6mr^2 + 9m^2 r - 4a^2 m\right)}{a^2 \left(2r^4 - 6m^2 r^2 + a^2 r^2 + 2a^2 mr + a^2 m^2\right)}. \tag{A.1}$$

By defining dimensionless variables, (2.14), mass parameter of the black hole can be eliminated from these equations,

$$\nu = -\frac{x^3 \left(x^3 - 6x^2 + 9x - 4u\right)}{u \left(2x^4 - 6x^2 + ux^2 + 2ux + u\right)}. \tag{A.2}$$

Finally, from this equation sextic polynomial can be obtained,

$$\begin{aligned} p(x) \quad \equiv \quad & x^6 - 6x^5 + (9 + 2\nu u)x^4 - 4ux^3 \\ & -\nu u(6 - u)x^2 + 2\nu u^2 x + \nu u^2 = 0. \end{aligned} \tag{A.3}$$

APPENDIX B

ABEL-RUFFINI THEOREM

Abel-Ruffini theorem (or Abel-Ruffini impossibility theorem) states that a polynomial of the form

$$p(x) = x^n + c_1 x^{n-1} + c_2 x^{n-2} + \cdots + c_n, \tag{B.1}$$

where $c_n \in \mathbb{Q}$, cannot be solved in terms of finite numbers of radicals for $n > 4$ [48]. In other words, it is impossible to find a general formula by using elementary operations, $(+, -, /, \times, \sqrt{})$, and coefficients of the polynomial, $c_1, c_2, \ldots, c_n$, which solves a polynomial of degree $n > 4$ [49]. For a detailed proof of this theorem, see [48]

In 1799, Paolo Ruffini published a paper and showed the unsolvability of quintic equations. But his proof was incomplete. A complete proof was provided by Niels Henrik Abel in 1824 and he extended his proof in a paper published in 1826. A complete treatment for all equations with any order provided by Evoriste Galois in 1830. Today, the proof of this theorem in most of the standard textbooks provided with the Galois theory [49].

APPENDIX C

TSCHIRNHAUSEN TRANSFORMATION AND NESTED RADICALS

As already established, there are no known exact solutions in terms of finite number of radicals to the polynomials with order $n > 4$. That is why approximate solutions are essential to understand the roots of the sextic equation (2.15). The complicated form of the (2.15) can be converted into simpler and more convenient form via Tschirnhausen transformation. By this way, an approximate solution in the nested radicals form can be provided.

Tschirnhausen transformations were introduced by the German mathematician Ehrenfried von Tschirnhaus in a paper published in 1683 [50]. This method says that, a polynomial in the form

$$x^n + p_1 x^{n-1} + p_2 x^{n-2} + ... + p_n = 0 \tag{C.1}$$

can be transformed into

$$y^n + q_1 y^{n-1} + q_2 y^{n-2} + ... + q_n = 0 \tag{C.2}$$

via the equation of the form

$$y = \alpha x^4 + \beta x^3 + \gamma x^2 + \delta x + \epsilon, \tag{C.3}$$

where the coefficients $q_1, q_2, q_3, \ldots$ are homogeneous functions of degrees $1, 2, 3, \ldots$ in $\alpha, \beta, \gamma, \delta, \epsilon$ and the first three coefficients of the transformed polynomial can be made zero ($q_1 = 0, q_2 = 0, q_3 = 0$) by judiciously chosen coefficients $(\alpha, \beta, \gamma, \delta, \epsilon)$ of the transforming equation (For a detailed proof of this statement, see [51]). The method works as follows. First, an ϵ value which makes $q_1 = 0$ has to be found and be substituted into the equations $q_2 = 0$ and $q_3 = 0$. $q_2 = 0$ is an homogeneous equation of order 2 in α, β, γ and δ. Then, this equation can be written in the form of sum of

n squares (For a detailed proof of this proposition, see [51]). Due to the fact that the equation admits four variables, $n = 4$, it can be written as

$$q_2 = a^2 - b^2 + c^2 - d^2. \tag{C.4}$$

Now, by choosing $a = b$ and $c = d$, q_2 can be made zero. These two equalities help to find linear relationships between the remaining four coefficients such that

$$\gamma = a_1\alpha + b_1\beta, \tag{C.5}$$

$$\delta = a_2\alpha + b_2\beta. \tag{C.6}$$

By substituting these γ and δ values into the equation $q_3 = 0$, a cubic equation of $\frac{\beta}{\alpha}$ can be obtained. With these relations at hand, by assigning a particular value to any one of the coefficients, other coefficients can be calculated accordingly. This completes the transformation.

At this point, thanks to the Tschirnhausen transformation, the sextic equation (2.15) is converted into a simpler sextic equation in the form

$$y^6 + ay^2 + by + c = 0. \tag{C.7}$$

This equation can be written and solved in the form, [52],

$$y^6 + a\left(y + \frac{b}{2a}\right)^2 + c - \frac{b^2}{4a} = 0, \tag{C.8}$$

$$a\left(y + \frac{b}{2a}\right)^2 = -y^6 + \frac{b^2}{4a} - c, \tag{C.9}$$

$$\left(y + \frac{b}{2a}\right)^2 = \frac{-y^6 + \frac{b^2}{4a} - c}{a}, \tag{C.10}$$

$$\left(y + \frac{b}{2a}\right)^2 = -\frac{y^6}{a} + \frac{\Delta}{4a^2}, \tag{C.11}$$

$$y + \frac{b}{2a} = \sqrt{-\frac{y^6}{a} + \frac{\Delta}{4a^2}}, \tag{C.12}$$

$$y = -\frac{b}{2a} + \sqrt{-\frac{y^6}{a} + \frac{\Delta}{4a^2}}. \tag{C.13}$$

The final equation can be written in the nested form

$$y = -\frac{b}{2a} + \sqrt{\frac{\Delta}{4a^2} - \frac{1}{a}\left(-\frac{b}{2a} + \sqrt{\frac{\Delta}{4a^2} - \ldots}\right)^6}. \tag{C.14}$$

Unfortunately, calculating this approximate result required an excess of computational power. Therefore, an exemplary approximate result cannot be provided in here.

APPENDIX D

DISCRIMINANT OF A POLYNOMIAL

For a polynomial of the form

$$p(x) = a_n x^n + a_{n-1} x^{n-1} + \cdots + a_1 x + a_0, \tag{D.1}$$

where $n > 0$, the discriminant can be defined as

$$\mathcal{D} = a_n^{2n-2} \prod_{i,j}^{n} (r_i - r_j)^2 , \tag{D.2}$$

for $i < j$, where r_i's are roots of the polynomial. The discriminant vanishes only when two or more roots are equal, as can be observed from the definition.

The discriminant of a polynomial of the form

$$p(x) = x^n + a_{n-1} x^{n-1} + \cdots + a_1 x + a_0, \tag{D.3}$$

where $n > 0$, can also be defined as

$$\mathcal{D} = (-1)^{\frac{n(n-1)}{2}} \mathcal{R}\left(p(x), p'(x)\right) \tag{D.4}$$

where $\mathcal{R}$ is the resultant [53].

APPENDIX E

DERIVATION OF THE CRITICAL ANGLE

According to Descartes' rule of sign, there should be 4, 2 or 0 positive roots. With the help of the discriminant of the sextic polynomial equation with respect to x, the point in the $(u,\ \nu)$ parameter space where the number of real roots reduces from four to two can be decided. This point is important because it is possible to factor the sextic polynomial equation into a quadratic part and a quartic part.

After making the following simplifications

$$u \equiv 1 - w^3, \qquad \nu \equiv \frac{\xi}{u}, \tag{E.1}$$

the sextic polynomial equation becomes

$$\begin{aligned} p(x) \;=\;& x^6 - 6x^5 + x^4 (2\xi + 9) + x^3 \left(4w^3 - 4\right) - x^2 \left(\xi w^3 + 5\xi\right) \\ & + x \left(2\xi - 2\xi w^3\right) + \xi - \xi w^3. \end{aligned} \tag{E.2}$$

The discriminant of the sextic polynomial equation with respect to x becomes

$$\begin{aligned} \mathcal{D} \;=\;& 4096\xi^2(\xi + 27)w^3 \left(w^3 - 1\right) \left(\xi + w^3 - 1\right)^3 \\ & \big((7\xi - 3)^3 + (\xi(\xi(\xi + 18) - 54) - 81)w^6 \\ & + (\xi(594 - \xi(20\xi + 63)) + 81)w^3 + 27w^9\big)\,. \end{aligned} \tag{E.3}$$

This discriminant value vanishes, $\mathcal{D} = 0$, at

$$\xi_{\text{cr}} = \frac{3(1 - w)^3}{7 + (w - 5)w}. \tag{E.4}$$

Due to the fact that ξ_{cr} is a single root of the discriminant equation, there is a sign change occuring around this point and, therefore, there will be four real roots of the sextic polynomial for ξ values above the ξ_{cr} and two real roots for ξ values below the ξ_{cr}.

APPENDIX F

LAGRANGE-BÜRMANN THEOREM

Lagrange-Bürmann theorem (or Lagrange-Bürmann inversion theorem) is a Taylor series expansion of the inverse of an analytical function. The theorem first published by Joseph-Louis Lagrange in 1770 [54]. Then, it was generalized by Hans Heinrich Bürmann in 1799 [55].

Assume that there is an analytic function, f, of the form

$$\omega = f(z), \tag{F.1}$$

where $\omega, z \in \mathbb{C}$. Assume also that there is point z_0 at which the function is analytical,

$$\omega_0 = f(z_0), \tag{F.2}$$

and has a non-vanishing first derivative,

$$\left.\frac{df}{dz}\right|_{z=z_0} \neq 0. \tag{F.3}$$

Let g be a function defined as the inverse of the function f,

$$z = g(\omega). \tag{F.4}$$

Lagrange-Bürmann theorem states that the inverse function can be expanded as

$$g(z) = \omega_0 + \sum_{n=1}^{\infty} \omega_n \frac{(f(z) - f(z_0))^n}{n!}, \tag{F.5}$$

where the coefficients are given by

$$\omega_n = \lim_{z \to z_0} \frac{d^{n-1}}{dz^{n-1}} \left(\frac{z - z_0}{f(z) - f(z_0)} \right)^n \tag{F.6}$$

[55], [56].

APPENDIX G

EXPLICIT FORMS OF INVARIANTS OF THE WARPED AdS_3 BLACK HOLE

The explicit forms of the curvature invariants calculated for the $t = t_0$ hypersurface of warped AdS_3 black hole are

$$
\begin{aligned}
{}^{\Sigma}I_3 \;=\; & -\frac{1}{\ell^6 r^6 \left(\left(\nu^2+3\right)(p+q) - 4\nu\sqrt{pq\left(\nu^2+3\right)} + 3r\left(\nu^2-1\right) \right)^6} \qquad \text{(G.1)} \\
& \times \left(\left(\nu^2+3\right)^3 (p-r)(r-q) \times \left(p^2 \left(\nu^2+3\right) \right.\right. \\
& \left(-4q^2 \left(2\nu\left(11\nu^2+9\right)\sqrt{pq\left(\nu^2+3\right)} + 9r\left(-3\nu^4+2\nu^2+1\right)\right)\right. \\
& -48qr\nu\left(\nu^2-1\right)\sqrt{pq\left(\nu^2+3\right)} + 3q^3\left(\nu^2+3\right)\left(17\nu^2+3\right) \\
& +24r^3\nu^2\left(\nu^2-1\right)\big) + 3p^3q\left(\nu^2+3\right)^2\left(-4\nu\sqrt{pq\left(\nu^2+3\right)} + p^4q\left(\nu^2+3\right)^3\right. \\
& +q\left(17\nu^2+3\right) + 2r\left(\nu^2-1\right)\big) + p\left(6q^3\left(\nu^2+3\right)^2\left(r\left(\nu^2-1\right)\right.\right. \\
& \left.-2\nu\sqrt{pq\left(\nu^2+3\right)}\right) - 48q^2r\nu\left(\nu^4+2\nu^2-3\right)\sqrt{pq\left(\nu^2+3\right)} \\
& +12r^3\nu\left(v^2-1\right)\left(3r\nu\left(\nu^2-1\right) - 2\left(5\nu^2+3\right)\sqrt{pq\left(\nu^2+3\right)}\right) \\
& \left.+q^4\left(\nu^2+3\right)^3 + 144qr^3\nu^2\left(\nu^4+2\nu^2-3\right)\right) \\
& +12r^3\nu\left(\nu^2-1\right)\left(-3r\left(\nu^2-1\right)\sqrt{pq\left(\nu^2+3\right)}\right. \\
& \left.\left.\left.-2q\left(5\nu^2+3\right)\sqrt{pq\left(\nu^2+3\right)} + 2q^2\nu\left(\nu^2+3\right) + 3qr\nu\left(\nu^2-1\right)\right)\right)^2\right),
\end{aligned}
$$

and

$$
\begin{aligned}
{}^{\Sigma}I_5 \;=\; & -\frac{1}{\ell^{10}r^{10}\left(\left(\nu^2+3\right)(p+q)-4\nu\sqrt{pq\left(\nu^2+3\right)}+3r\left(\nu^2-1\right)\right)^{10}} \qquad \text{(G.2)}\\
& \times\left(4\left(\nu^2+3\right)^5(p-r)(r-q)\times\left(2p^2\left(\nu^2+3\right)\left(-4q\nu\sqrt{pq\left(\nu^2+3\right)}\right.\right.\right.\\
& +q^2\left(9\nu^2+3\right)+2r^2\left(2\nu^2-3\right)\big)+p^3q\left(\nu^2+3\right)^2\\
& +4r^2\left(q\left(\nu\left(15-7\nu^2\right)\sqrt{pq\left(\nu^2+3\right)}-18r\left(\nu^2-1\right)\right)\right.\\
& -9r\left(\nu^2-1\right)\left(r\left(\nu^2-1\right)-2\nu\sqrt{pq\left(\nu^2+3\right)}\right)\\
& +q^2\left(2\nu^4+3\nu^2-9\right)\big)+pq^3\left(\nu^2+3\right)^2-24pqr^2\left(\nu^2+3\right)\\
& +4pr^2\left(\nu\left(15-7\nu^2\right)\sqrt{pq\left(\nu^2+3\right)}-18r\left(\nu^2-1\right)\right)\\
& -8q\nu\left(pq\left(\nu^2+3\right)\right)^{3/2}\Big)^2\left(p^2\left(\nu^2+3\right)\left(-4q^2\left(2\nu\left(11\nu^2+9\right)\sqrt{pq\left(\nu^2+3\right)}\right.\right.\right.\\
& +9r\left(-3\nu^4+2\nu^2+1\right)\big)-48qr\nu\left(\nu^2-1\right)\sqrt{pq\left(\nu^2+3\right)}\\
& +3q^3\left(\nu^2+3\right)\left(17\nu^2+3\right)+24r^3\nu^2\left(\nu^2-1\right)\big)\\
& +3p^3q\left(\nu^2+3\right)^2\left(-4\nu\sqrt{pq\left(\nu^2+3\right)}+q\left(17\nu^2+3\right)+2r\left(\nu^2-1\right)\right)\\
& +p^4q\left(\nu^2+3\right)^3+p\left(6q^3\left(\nu^2+3\right)^2\left(r\left(\nu^2-1\right)-2\nu\sqrt{pq\left(\nu^2+3\right)}\right)\right.\\
& -48q^2r\nu\left(\nu^4+2\nu^2-3\right)\sqrt{pq\left(\nu^2+3\right)}\\
& +12r^3\nu\left(v^2-1\right)\left(3r\nu\left(\nu^2-1\right)-2\left(5\nu^2+3\right)\sqrt{pq\left(\nu^2+3\right)}\right)\\
& +q^4\left(\nu^2+3\right)^3+144qr^3\nu^2\left(\nu^4+2\nu^2-3\right)\Big)\\
& +12r^3\nu\left(\nu^2-1\right)\left(-3r\left(\nu^2-1\right)\sqrt{pq\left(\nu^2+3\right)}\right.\\
& \left.\left.\left.-2q\left(5\nu^2+3\right)\sqrt{pq\left(\nu^2+3\right)}+2q^2\nu\left(\nu^2+3\right)+3qr\nu\left(\nu^2-1\right)\right)\right)^2\right).
\end{aligned}
$$

APPENDIX H

EXPLICIT FORMS OF INVARIANTS OF THE KERR BLACK HOLE

The explicit forms of the curvature invariants calculated for the $X(p) = X_0 =$ constant hypersurface of Kerr black hole are

$$\begin{aligned} {}^{\Sigma}I_1 \;=\; & \frac{1}{\left(a^2X_0^2+r^2\right)^6} \times \Big(4\left(a^4rX_0^4\left(r\left(46m^2-10mr+r^2\right)-14a^2m\right)\right. \\ & \left.+2a^2mr^3X_0^2\left(3a^2+r(r-16m)\right)+2a^6rX_0^6(4m+r)+a^8X_0^8+6m^2r^6\right)\Big)\,, \end{aligned} \tag{H.1}$$

and

$$\begin{aligned} {}^{\Sigma}I_5 \;=\; & \frac{1}{\left(a^2X_0^2+r^2\right)^{15}} \times \Big(64\left(a^2+r(r-2m)\right)\left(a^6X_0^6\left(7a^2m\right.\right. \\ & \left.+r\left(-46m^2+59mr+8r^2\right)\right)+2a^4r^2X_0^4\left(r\left(147m^2\right.\right. \\ & \left.\left.-25mr+2r^2\right)-43a^2M\right)+a^2mr^4X_0^2\left(27a^2+r(7r-146m)\right) \\ & \left.+4a^8X_0^8(r-m)+18m^2r^7\right)^2\Big)\,. \end{aligned} \tag{H.2}$$

APPENDIX I

EXPLICIT FORMS OF INVARIANTS OF THE 4+1 MYERS-PERRY HOLE

The explicit forms of the curvature invariants calculated for the $X_0 =$ constant hypersurface of 4+1 Myers-Perry black hole are

$$\begin{aligned} {}^{\Sigma}I_1 \;=\; & \frac{1}{\left(X_0^2(k-l)(k+l)+l^2+r^2\right)^6} \times \left(4\left(\left(2r^2\left(k^2+l^2-6m\right)\right.\right.\right. \\ & -6k^2m+k^4-6l^2m+l^4+5m^2+2r^4\Big) \\ & \times\left(X_0^2(k-l)(k+l)+l^2+r^2\right)^2-2\left(k^2+l^2-m+2r^2\right) \\ & \times\left(X_0^2(k-l)(k+l)+l^2+r^2\right)^3+6m\left(2r^2\left(k^2+l^2-m\right)\right. \\ & \left.+k^2l^2+3r^4\right)\left(X_0^2(k-l)(k+l)+l^2+r^2\right) \\ & -10k^2l^2mr^2-10k^2mr^4+3\left(X_0^2(k-l)(k+l)+l^2+r^2\right)^4 \\ & \left.\left.-10l^2mr^4+21m^2r^4-10mr^6\right)\right), \end{aligned} \tag{I.1}$$

and

$$\begin{aligned} {}^{\Sigma}I_5 \;=\; & \frac{1}{\left(X_0^2(k-l)(k+l)+l^2+r^2\right)^{15}} \times \left(256\left(\left(k^2+r^2\right)\left(l^2+r^2\right)-mr^2\right)\right. \\ & \times\left(2\left(r^2\left(2\left(k^2+l^2\right)-21m\right)-9k^2m+k^4-9l^2m+l^4+8m^2+2r^4\right)\right. \\ & \left(X_0^2(k-l)(k+l)+l^2+r^2\right)^2-\left(4k^2+4l^2-9m+8r^2\right) \\ & \times\left(X_0^2(k-l)(k+l)+l^2+r^2\right)^3+m\left(r^2\left(40\left(k^2+l^2\right)-51m\right)\right. \\ & \left.+20k^2l^2+60r^4\right)\left(X_0^2(k-l)(k+l)+l^2+r^2\right) \\ & -3mr^2\left(10k^2\left(l^2+r^2\right)+r^2\left(10l^2-21m+10r^2\right)\right) \\ & \left.\left.+5\left(X_0^2(k-l)(k+l)+l^2+r^2\right)^4\right)^2\right). \end{aligned} \tag{I.2}$$